bioRxiv preprint doi: https://doi.org/10.1101/2020.08.17.253716; this version posted August 17, 2020. The copyright holder for this preprint (which was not certified by peer review) is the author/funder, who has granted bioRxiv a license to display the preprint in perpetuity. It is made available under aCC-BY-NC-ND 4.0 International license.

New insights into *Cryptococcus* extracellular vesicles suggest a new structural model and an antifungal vaccine strategy

Juliana RIZZO[1#], Sarah Sze Wah WONG[2], Anastasia D. GAZI[3], Frédérique MOYRAND[1#], Thibault CHAZE[4], Pierre-Henri COMMERE[5], Sophie NOVAULT[5], Mariette MATONDO[4], Gerard PEHAU-ARNAUDET[3], Flavia C. G. REIS[6,7#], Matthijn VOS[8], Lysangela R ALVES[6#], Robin C. MAY[9#], Leonardo NIMRICHTER[10#], Marcio L. RODRIGUES[6,10#], Vishukumar AIMANIANDA[2] and Guilhem JANBON[1#*]

[1] Unité Biologie des ARN des Pathogènes Fongiques, Département de Mycologie, Institut Pasteur, F-75015, Paris, France
[2] Unité Mycologie Moléculaire, CNRS UMR2000, Département de Mycologie, Institut Pasteur, F-75015, Paris, France
[3] Ultrastructural Bio-Imaging, UTechS UBI, Département de Biologie cellulaire et infection, UMR 3528 CNRS, Institut Pasteur, F-75015, Paris, France
[4] Plateforme Protéomique, Unité de Spectrométrie de Masse pour la Biologie (MSBio), Centre de Ressources et Recherches Technologiques (C2RT), UMR 2000 CNRS, Institut Pasteur, Paris, France
[5] Cytometry and Biomarkers, Centre de Ressources et Recherches Technologiques (C2RT), Institut Pasteur, F-75015, Paris, France
[6] Instituto Carlos Chagas, Fundação Oswaldo Cruz (FIOCRUZ), Curitiba, Brazil
[7] Centro de Desenvolvimento Tecnologico em Saude (CDTS-Fiocruz), Brazil
[8] NanoImaging Core Facility, Centre de Ressources et Recherches Technologiques (C2RT), Institut Pasteur, F-75015, Paris, France
[9] Institute of Microbiology and Infection and School of Biosciences, University of Birmingham, Birmingham B15 2TT, United Kingdom
[10] Instituto de Microbiologia Paulo de Góes (IMPG), Universidade Federal do Rio de Janeiro, Rio de Janeiro, Brazil

[#] Members of the data sharing transparency group on fungal extracellular vesicles
* Corresponding author: janbon@pasteur.fr

bioRxiv preprint doi: https://doi.org/10.1101/2020.08.17.253716; this version posted August 17, 2020. The copyright holder for this preprint (which was not certified by peer review) is the author/funder, who has granted bioRxiv a license to display the preprint in perpetuity. It is made available under aCC-BY-NC-ND 4.0 International license.

Abstract

Whereas extracellular vesicle (EV) research has become commonplace in different biomedical fields, this field of research is still in its infancy in mycology. Here we provide a robust set of data regarding the structural and compositional aspects of EVs from the pathogenic yeast *C. neoformans*. By using cutting-edge methodological approaches including cryogenic electron microscopy and cryogenic electron tomography, proteomics, and nanoscale flow cytometry, we revisited cryptococcal EV features and suggest a new EV structural model, in which the vesicular lipid bilayer is covered by a 16 nm thick mannoprotein-based fibrillar decoration, bearing the capsule polysaccharide as its outer layer. About 10% of the EV population is devoid of fibrillar decoration, adding another aspect to EV diversity. By analyzing EV protein cargo from three cryptococcal species, we characterized the typical *Cryptococcus* EV proteome. It contains several membrane-bound protein families, including some Tsh proteins bearing a SUR7/PalI motif. The presence of known protective antigens on the surface of *Cryptococcus* EVs, resembling the morphology of encapsulated virus structures, suggested their potential as a vaccine. Indeed, mice immunized with EVs obtained from an acapsular *C. neoformans* mutant strain rendered a strong antibody response and significantly prolonged survival of mice upon *C. neoformans* infection.

Keywords: *Cryptococcus,* fungal infections, extracellular vesicles, mannoproteins, vaccine; Cryo-EM

bioRxiv preprint doi: https://doi.org/10.1101/2020.08.17.253716; this version posted August 17, 2020. The copyright holder for this preprint (which was not certified by peer review) is the author/funder, who has granted bioRxiv a license to display the preprint in perpetuity. It is made available under aCC-BY-NC-ND 4.0 International license.

1. Introduction

All living organisms release lipid bilayer-delimited particles defined as extracellular vesicles (EVs) (Deatherage and Cookson 2012, Witwer and Théry 2019). EV sizes range from 20 nm to close to one micrometer in diameter. In mammalian cells, two major classes of EVs have been defined, microvesicles and exosomes, according to their size and cellular origin (Meldolesi 2018, van Niel et al. 2018). In these organisms, a large body of literature describes how EVs participate in intercellular signaling within an organism but also in organism-to-organism communication, including carcinogenesis and host-pathogen interactions (Xu et al. 2018, Shopova et al. 2020). In fungi, the first report of fungal EVs was published in 2007 (Rodrigues et al. 2007), and, since then, their existence has been reported in many species of pathogenic and nonpathogenic fungi (Rizzo et al. 2020).

By analogy with mammalian EVs, it has been hypothesized that fungal EVs could also participate in many biological processes (Rodrigues and Casadevall 2018). Indeed, some reports indicate their relevance in diverse mechanisms related to fungal pathophysiology, such as antifungal resistance and biofilm formation (Leone et al. 2018, Zarnowski et al. 2018), transfer of virulence-associated molecules and modulation of host cells (Oliveira et al. 2010, Vargas et al. 2015, Rizzo et al. 2017, Bielska et al. 2018, Souza et al. 2019, Hai et al. 2020), cell wall remodeling and biogenesis (Zhao et al. 2019, Rizzo et al. 2020), among others (Bielska and May 2019, Rizzo et al. 2020). Nevertheless, the molecular mechanisms implicated in these exchanges of information, as well as the genetics regulating fungal EV biogenesis and release, remain elusive.

As with their mammalian, bacterial and plant counterparts, fungal EVs have been shown to contain proteins, pigments, nucleic acids, polysaccharides, lipids, among other molecules (Eisenman et al. 2009, Vallejo et al. 2012, da Silva et al. 2015, Rodrigues et al. 2015, Joffe et al. 2016, Rayner et al. 2017). Besides the claudin-like Sur7 family proteins, recently suggested as EV protein markers in *Candida albicans* (Dawson et al. 2020), no other fungal EV specific molecular marker has been reported. Indeed, the laborious and inefficient EV isolation protocols that have been used until recently have strongly limited the knowledge on their composition. Additional hurdles regarding purification methods can possibly affect an accurate vesicular compositional characterization (Théry et al. 2018), including potential carryover contaminants such as protein aggregates (Chiou et al. 2018). Regarding EV morphological diversity, previous studies have reported the heterogeneity of fungal EV size, as recently reviewed (Bielska and May 2019). However, single particle analyzers such as the widely used Nanoparticle Tracking Analysis (NTA) and most common flow cytometers cannot reliably

bioRxiv preprint doi: https://doi.org/10.1101/2020.08.17.253716; this version posted August 17, 2020. The copyright holder for this preprint (which was not certified by peer review) is the author/funder, who has granted bioRxiv a license to display the preprint in perpetuity. It is made available under aCC-BY-NC-ND 4.0 International license.

evaluate particles smaller than 100 nm in diameter (Maas et al. 2015, Théry et al. 2018, Chiang and Chen 2019, Noble et al. 2020). Overall, although a considerable number of fungal EV-related studies have been published in recent years, our knowledge of fungal EV structure and composition remains limited, which prevents further robust analysis of their functions.

C. neoformans is a major fungal pathogen, affecting mostly immunocompromised patients (Rajasingham et al. 2017) and has historically been the one of the most studied fungi regarding EV biology (Rodrigues et al. 2007, Bielska and May 2019, Rizzo et al. 2020). However, the only structural analyses of EVs from this organism are now very outdated and technologies used have shown tremendous improvements since then (Emelyanov et al. 2020, Noble et al. 2020). Additionally, so far *Cryptococcus* EV proteomics identified only 92 and 202 proteins, with very poor overlap and no evaluation of their abundance or enrichment (Rodrigues et al. 2008, Wolf et al. 2014). Finally, although the current model of fungal EV structure contains proteins located on the vesicular surface (by analogy with the mammalian EV structures (Emelyanov et al. 2020, Noble et al. 2020)), more experimental evidence is necessary to identify these putative membrane-associated molecules in fungal EVs.

Since many immunogenic proteins are often found to be associated with EVs, their vaccine potential has been explored mostly for bacterial and parasitic infections (Coakley et al. 2017, Wang et al. 2018), and more recently also for fungal infections (Colombo et al. 2019, Vargas et al. 2020). In the present study, we used the recently described protocol (Reis et al. 2019), to obtain EV- enriched samples from *Cryptococcus* cells, together with cutting edge methodological approaches to revisit *Cryptococcus* EV structure, cargo, and biological functions. We produced a robust set of data containing cryo-electron microscopy (cryo-EM) and cryo-electron tomography (cryo-ET) proteomics, and nanoscale flow cytometry analysis, suggesting a new EV structural model, in addition to a list of cryptococcal EV protein markers. Our results led us to evaluate the EV biological roles in mice models further, emphasizing their potential use as an anti-cryptococcosis vaccine.

2. Material and Methods

Strains and media

The wild type strains used in the study were *C. neoformans* strain KN99α, *C. deneoformans* strain JEC21, *C. deuterogattii* strain R265, *C. albicans* strain SC5314, and *S. cerevisiae* strain S288C. To construct the strains NE1281 and NE1282 (*MATα mp88Δ::NEO*) the entire

bioRxiv preprint doi: https://doi.org/10.1101/2020.08.17.253716; this version posted August 17, 2020. The copyright holder for this preprint (which was not certified by peer review) is the author/funder, who has granted bioRxiv a license to display the preprint in perpetuity. It is made available under aCC-BY-NC-ND 4.0 International license.

CNAG_03223 CDS was replaced by the NEO marker in KN99α following the previously described CRISPR CAS9 method (Fan and Lin 2018). The plasmid pPZP-NEO1 used to amplify the *NEO* selective marker was kindly provided by Dr. Joseph Heitman (Duke University). The deletion cassettes as constructed using a strategy previously applied to *Neurospora crassa* (Collopy et al. 2010). The transformants were then screened for homologous integration, as previously described (Moyrand et al. 2007). Two representatives independently obtained mutant strains were stocked at -80°C. All primer sequences used are provided in Table S3. The *vep1Δ::NAT* (CNAG_03223) has been constructed Hiten Madhani lab (UCSF, USA) obtained from the Fungal Genetic stock center. All strains were taken from the G. Janbon laboratory collection at -80°C, plated on yeast extract-peptone-dextrose (YPD) and incubated at 30°C for 48h before each experiment.

EV isolation and labeling

EV purification was based on the recently published protocol (Reis et al. 2019) with some modifications. One loop of cells was inoculated into 10 mL of liquid YPD and incubated at 30°C for 24h with shaking (150rpm). Cells were washed two times with 10 ml of sterile water, counted and diluted to a density of $3.5x10^7$cells/mL in water. Aliquots of 300 µL of the cellular suspension were spread onto synthetic dextrose (SD) solid medium plates and incubated for 24h at 30°C to reach cell confluence. The cells were recovered from each plate with a 10µL inoculation loop and transferred to an ultracentrifugation tube containing 10 mL 0.22 µm-filter sterile PBS 0.01M. Cells were homogenized and collected by centrifugation at 5,000 x g for 15 min at 4ºC. Supernatants were collected and centrifuged again at 15,000 x g for 15 min at 4ºC to eliminate cellular debris. The resting supernatants were filtered at 0.45µm syringe filters and ultracentrifuged at 100.000 x g for 1h at 4°C (SW 41 Ti swinging-bucket rotor, Beckman Coulter). The supernatant was discarded and pellets suspended in 0.22 µm-pore filtered or 0.02 µm-pore filtered (in case of Flow Cytometry analysis) PBS for immediately use, or stored at -80°C for further experiments.

EVs were obtained as previously described and finally suspended in 100 µL of 0.02 µm-pore filtered PBS. EVs were labeled either with the Concanavalin A (ConA) - Alexa Fluor™ 488 conjugated, or with the Alexa 488 labeled anti-GXM monoclonal antibody 18B7 (Casadevall et al. 1992), a kind gift of Oscar Zaragoza. The ConA stock solution (5mg/mL) was previously centrifuged at 13.000 x rpm for 2 min, in order to eliminate possible aggregates, and diluted to 500µg/mL in filtered PBS. In 1.5 mL Eppendorf tubes, 5 µL of ConA (500 µg/mL), together with 5µL EV suspension were add to a final volume of 200µL filtered PBS.

bioRxiv preprint doi: https://doi.org/10.1101/2020.08.17.253716; this version posted August 17, 2020. The copyright holder for this preprint (which was not certified by peer review) is the author/funder, who has granted bioRxiv a license to display the preprint in perpetuity. It is made available under aCC-BY-NC-ND 4.0 International license.

The tubes were incubated for one hour at 30°C, under agitation and protected from light. After incubation, 200 µL of 0.02 µm-pore filtered PBS were added to each tube and 300 µL of the final suspension was transferred to BD Trucount™ Tubes (BD Biosciences) and proceeded to Flow Cytometry analysis. Similar protocol was applied for the EV labeling with the Alexa 488 labeled anti-GXM monoclonal antibody 18B7, which was diluted 20 times before adding to EV suspension.

Flow cytometry

EV were analyzed and sorted on a cell sorter MoFlo Astrios (Beckman Coulter) equipped with an EQ module specifically developed to detect nanoparticles and with 488 nm and 561 nm lasers at 200 mW. The sorting was carried out with a 70 µm nozzle at a pressure of 60 PSI and a differential pressure with the sample of 0.3-0.4 PSI. The sheath liquid NaCl 0.9% (REVOL, France) was filtered on a 0.04 µm filter. The analyses were on the SSC parameter of laser 561, with threshold set to 0.012% in order to have maximum 300 eps. An M2 mask was added in front of the FSC. All SSC and FSC parameters are viewed in logarithmic mode. The calibration of the machine was carried out using Megamix-Plus SSC beads from BioCytex. We used the Trucount™ Tubes to normalize the EV counting for ConA labeling, and the fluorescence of the Mab18B7 and alexa 488 conjugated, and beads Trucount™ was measured on parameter 488-513/26.

Nanoparticle tracking analysis (NTA)

Quantitative determination of EV size distribution was performed by NTA, in addition to microscopic methods. Protocols that were recently established for analysis of cryptococcal vesicles were used (ref Reis 2019, already in the reference list). Briefly, ultracentrifugation pellets were 20- to 50-fold diluted in filtered PBS and measured within the optimal dilution range of 9×10^7 to 2.9×10^9 particles/ml on an LM10 nanoparticle analysis system, coupled with a 488-nm laser and equipped with an SCMOS camera and a syringe pump (Malvern Panalytical, Malvern, United Kingdom). The data were acquired and analyzed using the NTA 3.0 software (Malvern Panalytical).

Cryo-EM and cryo-ET

Four microliters of EV samples, obtained from 24 plates of *C. neoformans* WT, were spotted on glow-discharged lacey grids (S166-3, EMS). The samples were cryo-fixed by plunge freezing at -180°C in liquid ethane using a Leica EMGP (Leica, Austria). Grids were observed

bioRxiv preprint doi: https://doi.org/10.1101/2020.08.17.253716; this version posted August 17, 2020. The copyright holder for this preprint (which was not certified by peer review) is the author/funder, who has granted bioRxiv a license to display the preprint in perpetuity. It is made available under aCC-BY-NC-ND 4.0 International license.

either with Tecnai F20, or Titan Krios (Thermo Fisher Scientific). The Tecnai F20 (Thermo Fisher Scientific) was operating at 200kV and images were acquired under low-dose conditions using the software EPU (Thermo Fisher Scientific) and a direct detector Falcon II (Thermo Fisher Scientific).

Cryo electron tomography was performed using 5 nm protein A gold particles (UMC, Utrecht). These were mixed with the sample to serve as fiducial markers for subsequent image alignment. 4 µl of sample was applied to glow discharged Lacey grids (S166-3, EMS) prior plunge-freezing (EMGP, Leica). Initial bi-directional tilt series acquired using a TECNAI F20 transmission electron microscope (FEI) operated at 200kV under parallel beam conditions using a Gatan 626 side entry cryoholder. The SerialEM software (Mastronarde 2005, Schorb et al. 2019) was used to automatically acquire images every 2° over a ±45° range using a Falcon II direct detector with a pixel size of 2 Å, using a total dose of 180 electrons per Å2.

Dose-symmetric tilt series were collected on a 300kV Titan Krios (Thermo Scientific) transmission electron microscope equipped with a Quantum LS imaging filter (Gatan, slit with 20 eV), single-tilt axis holder and K3 direct electron detector (Gatan). Tilt series with an angular increment of 2° and an angular range of ±60° were acquired with the Tomography software (Thermo Scientific). The total electron dose was between 120 and 150 electrons per Å2 and the pixel size at 3.38 Å. Dose symmetric tilt series were saved as separate stacks of frames and subsequently motion-corrected and re-stacked from −60° to +60° using IMOD's function align frames (Mastronarde and Held 2017) with the help of a homemade bash script.

Initial image shifts were estimated using IMOD's function tiltxcorr. Alignments were further optimized in IMOD using the tracing of 30-40 gold fiducials across the tilt series. The fiducial models gave an overall of a fiducial error around 6 ± 2.7 Å. In cases of a higher error, local alignments were taken into consideration, to further correct the sample's beam induced motion observed. Three-dimensional reconstructions were calculated in IMOD by weighted back projection using the SIRT-like radial filter to enhance contrast and facilitate subsequent segmentation analysis.

EV modeling and analysis of tomographic data

Tomograms were displayed and analyzed using the 3dmod interface of IMOD (Kremer et al. 1996). The vesicles were modeled with manual tracing of their great circle prior the use of the spherical interpolator of IMOD. If the elliptical contours calculated, could not follow adequately the vesicular membrane, further manual tracing was used before re-applying the interpolator. This involved tracing of membranes near the poles of the vesicles where the

bioRxiv preprint doi: https://doi.org/10.1101/2020.08.17.253716; this version posted August 17, 2020. The copyright holder for this preprint (which was not certified by peer review) is the author/funder, who has granted bioRxiv a license to display the preprint in perpetuity. It is made available under aCC-BY-NC-ND 4.0 International license.

membrane information could still be followed. To evaluate and assign diameters to a total of 434 regular vesicles, located in 39 tomograms, the value of the perimeter of the spheroid's great circle was extracted using the imodinfo function of IMOD, from the same initial manually traced contours used for modelling. To display in 3D the vesicle contour data were meshed using the imodmesh function of IMOD. The projections of the 3D spheroidal models were displayed and rotated to study their 3D geometry.

For the evaluation of the decoration thickness, 105 regular vesicles were analyzed by manually measuring the outer EV diameter (delimited by the fibrillar decoration) and the inner diameter (delimited by the lipid bilayer), across the longest axis of the vesicle. The final calculation of the decoration thickness was the subtraction of the inner diameter from the outer diameter, divided by two. For the modeling of the fibrillar decoration, the IMOD surface models were imported to UCSF Chimera (Pettersen et al. 2004). The models were used as masks to extract a slab of data around their outer surface, corresponding to the decoration. The thickness of the slab used refers to the mean value provided by the aforementioned manual analysis. Iso-surface representation of the decoration and final 3D data visualization of the models performed with UCSF Chimera (Pettersen et al. 2004).

Immunization assays

The animal experiments were approved by the ethical committee for animal experimentation Comité d'Éthique en Experimentation Animale (CETEA Project license number 2013-0055). Six-week old female BALB/C mice (Janvier Labs) were used in the two sets of vaccination assays. Three successive intraperitoneal injections (using either 1 or 10 µg of EVs-associated proteins in 100 µL) of 14-day intervals were given to the mice. Control group of mice was injected only with PBS. Blood was collected three-eleven days after the last immunization and tested for antibody response by Western blot. Briefly, the EVs-associated proteins were separated on 12% SDS-PAGE, and electroblotted to nitrocellulose membrane. By Western blotting, using the mouse sera at dilution 1:1000 and anti-mouse IgG antibody peroxidase conjugated (Sigma Aldrich), the antibody response specific to the EV-associated proteins was examined. Once the antibody response has been confirmed, all the immunized and control mice were challenged intranasally, around one month from the last immunization, with 10^4 cells of a wild-type *C. neoformans*, and the body weights and survival were monitored.

Vesicle denaturation and protein digestion

bioRxiv preprint doi: https://doi.org/10.1101/2020.08.17.253716; this version posted August 17, 2020. The copyright holder for this preprint (which was not certified by peer review) is the author/funder, who has granted bioRxiv a license to display the preprint in perpetuity. It is made available under aCC-BY-NC-ND 4.0 International license.

Protein samples were solubilized in urea 8 M, Tris 100 mM pH7.5, 5 mM tris (2-carboxyethyl) phosphine (TCEP) for 20 min at 23°C. Samples were sonicated using a Vibracell 75186 and a miniprobe 2 mm (Amp 80% // Pulse 10 off 0.8, 3 cycles). Proteins were then alkylated with 20 mM iodoacetamide for 30 min at room temperature in the dark. Subsequently, LysC (Promega) was added for the first digestion step (protein to Lys-C ratio = 80:1) for 3h at 30°C. Then samples were diluted down to 1 M urea with 100 mM Tris pH 7.5, and trypsin (Promega) was added to the sample at a ratio of 50:1 for 16h at 37°C. Proteolysis was stopped by adding Formic acid (FA) to a final concentration of 1 % (vol/vol). Resulting peptides were desalted using Sep-Pak SPE cartridge (Waters) according to manufactures instructions.

LC-MS/MS of tryptic digest

LC-MS/SM analysis of digested peptides was performed on an Orbitrap Q Exactive Plus mass spectrometer (Thermo Fisher Scientific, Bremen) coupled to an EASY-nLC 1200 (Thermo Fisher Scientific). A home-made column was used for peptide separation (C_{18} 40 cm capillary column picotip silica emitter tip (75 µm diameter filled with 1.9 µm Reprosil-Pur Basic C_{18}-HD resin, (Dr. Maisch GmbH, Ammerbuch-Entringen, Germany)). It was equilibrated and peptide was loaded in solvent A (0.1 % FA) at 900 bars. Peptides were separated at 250 $nl.min^{-1}$. Peptides were eluted using a gradient of solvent B (ACN, 0.1 % FA) from 3% to 22% in 160 min, 22% to 50% in 70 min, 50% to 90% in 5 min (total length of the chromatographic run was 250 min including high ACN level step and column regeneration). Mass spectra were acquired in data-dependent acquisition mode with the XCalibur 2.2 software (Thermo Fisher Scientific, Bremen) with automatic switching between MS and MS/MS scans using a top-10 method. MS spectra were acquired at a resolution of 70000 (at *m/z* 400) with a target value of 3×10^6 ions. The scan range was limited from 300 to 1700 *m/z*. Peptide fragmentation was performed using higher-energy collision dissociation (HCD) with the energy set at 27 NCE. Intensity threshold for ions selection was set at 1×10^6 ions with charge exclusion of z = 1 and z > 7. The MS/MS spectra were acquired at a resolution of 17500 (at *m/z* 400). Isolation window was set at 1.6 Th. Dynamic exclusion was employed within 45s.

Data processing

Data were searched using MaxQuant (version 1.5.3.8 and 1.6.6.0) (Cox and Mann 2008, Tyanova et al. 2016) using the Andromeda search engine (Cox et al. 2011) against home-made databases. The following databases were used. For *C. neoformans* KN99α, *C. deneoformans* JEC21 and *C. deuterogattii* R265 we used the recently updated proteomes (Ferrareze et al.

bioRxiv preprint doi: https://doi.org/10.1101/2020.08.17.253716; this version posted August 17, 2020. The copyright holder for this preprint (which was not certified by peer review) is the author/funder, who has granted bioRxiv a license to display the preprint in perpetuity. It is made available under aCC-BY-NC-ND 4.0 International license.

2020, Wallace et al. 2020). The following search parameters were applied: carbamidomethylation of cysteines was set as a fixed modification, oxidation of methionine and protein N-terminal acetylation were set as variable modifications. The mass tolerances in MS and MS/MS were set to 5 ppm and 20 ppm respectively. Maximum peptide charge was set to 7 and 7 amino acids were required as minimum peptide length. A false discovery rate of 1% was set up for both protein and peptide levels. The iBAQ intensity was used to estimate the protein abundance within a sample (Schwanhäusser et al. 2011).

Statistical analysis

All statistical analyses were performed using GraphPad Prism 8 software (GraphPad Software Inc.). Data sets were tested for normal distribution using Shapiro-Wilk or Kolmogorov-Smirnov normality tests. In the cases in which the data passed the normality test, they were further analyzed using the unpaired Student's t test. When at least one data set was nonnormally distributed, we used the nonparametric Kolmogorov-Smirnov test. For the comparison of the survival curves, we used the Logrank (Mantel-Cox) test.

3. Results

- ***Diversity of EVs produced by Cryptococcus***

Several groups have already performed morphological studies of fungal EVs by electron microscopy (Rodrigues et al. 2007, Oliveira et al. 2009, Rayner et al. 2017, Bleackley et al. 2020). However, most of these previous fungal EV structural analysis used sample fixation and dehydration procedures for transmission electron microscopy (TEM), which can often affect the size and morphology of EVs (Van Der Pol et al. 2010, Chiang and Chen 2019). Cryo-EM imaging on rapid freezing samples at low temperature could potentially reduce sample damaging and artifacts caused by the addition of heavy metals, dehydration, or fixation steps (Orlov et al. 2017, Chiang and Chen 2019). Indeed, diverse morphologies of EVs derived from even a single mammalian cell type have been clearly revealed under cryo-EM (Zabeo et al. 2017). We therefore used cryo-EM and cryo-ET in an effort to analyze EVs purified from *C. neoformans* cells, in their near-native state.

Based on the optimized version of the EV purification protocol recently described by Reis and collaborators (Reis et al. 2019), we isolated EVs from *C. neoformans* reference strain

bioRxiv preprint doi: https://doi.org/10.1101/2020.08.17.253716; this version posted August 17, 2020. The copyright holder for this preprint (which was not certified by peer review) is the author/funder, who has granted bioRxiv a license to display the preprint in perpetuity. It is made available under aCC-BY-NC-ND 4.0 International license.

KN99α, cultured on synthetic dextrose solid medium for 24h, in order to limit the carryover of potential contaminants. Cryo-ET tomograms allowed us to analyze 533 single vesicles, which were characterized according to their morphological aspects in regular (round-bilayered vesicles) and irregular (not rounded – bilayered or multilayered vesicles) categories. Although a large proportion (81.4%) of the observed EVs had the typical round shape, 18.6% corresponded to irregular morphologies. Among them, we observed examples of multilayer vesicles (1.7%), long tubular (2.3%), flat (4.7%), short tubular (6.9%), and miscellaneous morphologies (3.0%). The EV morphological diversity and distribution percentage in each subcategory are explored in **Fig. 1**.

Cryo-EM analysis showed a considerable polymorphism of EVs, with the two leaflets of the typical vesicular membrane readily visible for all EVs observed, and a few unstructured aggregates, thus confirming the quality of our preparation **(Fig. 2A).** Among the regular vesicles, only 10.8% appeared to have a smooth surface **(Fig. 2B and 2C)**; the majority of regular EVs (89.2%) were decorated with a fibrillar structure anchored to the lipid bilayer **(Fig. 2D and 2E).** Strikingly, regardless of the morphology, the majority of EVs analyzed (88.6%) appeared to be coated with this fibrillar material. We used the cryo-ET to prepare a three-dimensional surface model of the EVs, using the IMOD (Mastronarde and Held 2017) and UCSF Chimera (Pettersen et al. 2004) to further visualize their structure and fibrillar decoration **(Fig. 2F to 2H)**.

Additional aspects of *C. neoformans* EV diversity, such as the distribution of size and decoration, were analyzed. NTA analyses showed a diameter size distribution from 80 to 500 nm and revealed a major peak of vesicle detection in the 150-nm-diameter range **(Fig. 3A),** in line with previous findings (Reis et al. 2019)**.** We also analyzed the EV diameter frequency distribution by cryo-EM from the 434-single regular EV captures **(Fig. 3B)**. The size distribution of vesicles tracked with NTA was different from the distribution of vesicles observed with cryo-EM, which revealed a wider range of EV diameter size, ranging from as small as 10 nm to 500 nm **(Fig. 3C)**. Notably, smaller vesicles (< 100 nm) comprised a higher proportion of vesicles captured by cryo-EM than NTA. Although cryo-EM has some statistical limitations, it nonetheless confirms the known bias of NTA towards larger EVs (Bachurski et al. 2019).

Analysis of the EV size according to the presence or absence of the surface decoration revealed a different frequency distribution **(Fig. 3D)**, with non-decorated EVs showing a significantly smaller size distribution ($p=0.01$, using the nonparametric Kolmogorov-Smirnov test) compared to the decorated ones **(Fig. 3E).** Additionally, the analysis of the vesicular

bioRxiv preprint doi: https://doi.org/10.1101/2020.08.17.253716; this version posted August 17, 2020. The copyright holder for this preprint (which was not certified by peer review) is the author/funder, who has granted bioRxiv a license to display the preprint in perpetuity. It is made available under aCC-BY-NC-ND 4.0 International license.

decoration in 105 single regular EVs revealed heterogeneity in their thickness, ranging from 5 to 23 nm with the average value close to 16 nm **(Fig. 3F)**. There was no correlation between vesicular diameter size and decoration thickness, as indicated by linear regression analysis **(Fig. 3G).** Therefore, the presence or absence of decoration, and even its thickness, does not depend on the size and shape of the EVs, revealing a previously unknown aspect of fungal EV diversity.

- Cryptococcus EV structure analysis

C. neoformans is an encapsulated microorganism, and its capsule is mostly composed of the polysaccharide named glucuronoxylomannan (GXM), a critical virulence factor of this pathogenic yeast (O'Meara and Alspaugh 2012). GXM has been previously shown to be exported by EVs (Rodrigues et al. 2007). Therefore, we reasoned that the fibrillar decoration observed around the vesicles could be composed of this capsular polysaccharide. We thus incubated *C. neoformans* EVs with the Alexa 488 labeled anti-GXM monoclonal antibody 18B7 (Casadevall et al. 1992), and analyzed the EV suspension was by flow cytometry. More than 70% of the EVs obtained from the wild-type strain were recognized by this antibody **(Fig. 4A),** suggesting that most *C. neoformans* EVs are covered to some extent with GXM or derivatives thereof. While, EVs obtained from the acapsular mutant strain (*cap59Δ*) (Moyrand et al. 2007) were weakly labeled (2.33%), using the same experimental approach **(Fig. 4B)**. Nevertheless, cryo-EM observation of *cap59Δ* EVs revealed similar fibrils as observed in the wild type EVs **(Fig. 4B)**. Moreover, cryo-EM analysis of EVs purified from *cap59Δ* suggested a similar percentage of decorated EVs (91.6%). Overall, these data suggest that, even though GXM covers most *C. neoformans* EVs, the visible fibrillar structures around them are not GXM-based. Cryo-EM analysis of EVs obtained from *C. albicans* SC5314 and *S. cerevisiae* S288C grown on SD medium showed a similar fibrillar decoration we observed around *Cryptococcus* EVs **(Fig. 4C)**, reinforcing the notion that this structure is not GXM-based, since neither of these two yeasts can synthesize this capsular polysaccharide.

We then reasoned that EV decoration might be protein-based and therefore performed proteomic analyses to further explore this novel fungal vesicular feature. Two proteomic analyses of *C. neoformans* EVs have been reported previously (Rodrigues et al. 2008, Wolf et al. 2014) wherein the authors identified 92 and 202 proteins in *C. neoformans* EV extracts, respectively. However, neither quantitative nor enrichment of EV-associated proteins was performed in these two studies. Therefore, we performed EV proteomic characterization, together with an enrichment analysis in order to distinguish the proteins associated with EVs,

bioRxiv preprint doi: https://doi.org/10.1101/2020.08.17.253716; this version posted August 17, 2020. The copyright holder for this preprint (which was not certified by peer review) is the author/funder, who has granted bioRxiv a license to display the preprint in perpetuity. It is made available under aCC-BY-NC-ND 4.0 International license.

396 from the ones related to potential carryover aggregates, inevitably contaminating EV
397 preparations.

398 In fungi, and more specifically in *Cryptococcus*, the relationship between RNA and
399 protein abundances has been reported as nearly linear, due to the relatively minor contribution
400 of posttranscriptional regulations to protein abundance (Wallace et al. 2020). We thus used
401 cellular RNA abundance at 30°C, exponential phase (Wallace et al. 2020), as a proxy for
402 cellular protein abundance, and for normalization of EV proteome data. *C. neoformans* EVs
403 proteomic analysis was performed in experimental triplicate and produced a common list of
404 1847 proteins **(Table S1).**

405 Proteins were ranked according to their prevalence in the sample evaluating the average
406 intensity-based absolute quantification (IBAQ) value of the three replicates. We then used the
407 gene expression level as evaluate by RNA-seq analysis to calculate an enrichment coefficient
408 comparing the expected value in the cells with the observed one in EVs. We thus identified 39
409 non-ribosomal proteins which were present both within the 100 most prevalent EV proteins
410 overall and within the 100 most enriched proteins. We considered these proteins as EV-
411 associated proteins. Only 9 out of these 39 proteins were reported in previous proteomic
412 analysis, emphasizing the necessity for proteomic data enrichment analysis. Of note, our study
413 and those published before used different culture media, and distinct protocols of EV isolation,
414 which might also explain the differences in protein composition that were presently observed.

415 To further explore how conserved EV protein cargo is across *Cryptococcus* species, we
416 proceeded with the same strategy to characterize the EV-associated proteins in two other
417 cryptococcal species, *C. deneoformans* (strain JEC21) and *C. deuterogattii* (strain R265). We
418 identified 38 and 48 EV-associated proteins for *C. deneoformans* and *C. deuterogattii*,
419 respectively **(Table S2)**. Overall, 71 EV-associated proteins were identified, 37 in at least two
420 species, and 17 shared by all the three species **(Fig. 5A and B)**, supporting a conserved profile
421 of the EV-associated proteins across *Cryptococcus* species, and the robustness of our analyses.

422 Several families of proteins appeared to be typical of *Cryptococcus* EVs. The major one
423 was the Chitin deactelylase Cda family (Baker et al. 2011), composed of three members present
424 among the 17 EV-associated proteins identified in all *Cryptococcus* species analyzed. Some
425 other families like the putative glyoxal oxidase (Gox proteins), or the Ricin-type beta-trefoil
426 lectin domain-containing protein (Ril), have one member common to all three species EVs (i.e.
427 Gox2 and Ril1) whereas the other members are found in only two species (Ril2 and Ril3) or are
428 specific of one species EVs (Gox1 and Gox3) **(Fig. 5C)**. We also identified three tetraspanin
429 membrane proteins containing a SUR7/PalI family motif. Tsh1 and Tsh2 shared 32% of identity

bioRxiv preprint doi: https://doi.org/10.1101/2020.08.17.253716; this version posted August 17, 2020. The copyright holder for this preprint (which was not certified by peer review) is the author/funder, who has granted bioRxiv a license to display the preprint in perpetuity. It is made available under aCC-BY-NC-ND 4.0 International license.

in their amino acid sequence. Tsh1 is present in both *C. neoformans* and *C. deneoformans* EVs whilst Tsh2 was identified in both *C. neoformans* and *C. deuterogattii*. The third Sur7/PalI protein shares very little sequence homology beyond the SUR7 motif and is exclusive to *C. deuterogattii*. Two Sur7 proteins have been recently identified in *C. albicans* EVs, suggesting that they might represent a common EV marker present in fungal EVs (Dawson et al. 2020). Finally, two members of the previously described pr4/barwin domain Blp protein family (Chun et al. 2011) were present in *C. neoformans* and *C. deuterogattii* EVs but not in *C. deneoformans*. Similarly, the two ferroxidase Cfo proteins (Jung et al. 2008) were shown to be associated only with the *C. deuterogattii* EVs but not in the two other species.

Several enzymes associated with polysaccharide degradation and modifications were present in Cryptococcus EVs. Some of these proteins are specific of one species but some others are present in two or all three EV proteomes. For instance, the identification within the *Cryptococcus* EV core proteins of Gas1 (a 1,3-beta-glucanosyltransferase), Amy1 (an alpha amylase), Exg104 (a glucan 1,3-beta-glucosidase), Hep1 (a putative heparinase) together with the Gox, Cda and Ril proteins suggest functions of EVs in cell wall processes, as previously hypothesized in *S. cerevisiae* (Zhao et al. 2019). Finally, several of the EVs proteins identified here have no predicted function; we therefore named them Vep (Vesicles enriched protein).

Bioinformatics analysis of the 71 EV-associated protein sequences suggested that 80% might be membrane-bound, 36 of them bearing at least one putative transmembrane domain as predicted by SignalP-5.0 (Almagro Armenteros et al. 2019) and/or TMHMM v. 2.0 (Krogh et al. 2001), and 21 being putative GPI-anchored proteins as predicted by PredGPI (Pierleoni et al. 2008), which is in good agreement with putative protein-based decoration. Reflecting the general specificities of these three proteomes, the GPI-anchor EV-proteomes of *C. neoformans* and *C. deneoformans* are nearly identical, whereas *C. deuterogatii* is more diverse (**Fig. 5D**).

Mature GPI-anchored proteins can also be membrane-bound and are predicted to be highly mannosylated in *Cryptococcus* and other fungi (Levitz et al. 2001, de Groot et al. 2003). We thus reasoned that these mannosylated proteins might compose the EV decorations observed by cryo-EM. To test this hypothesis, we incubated EVs with the Concanavalin A (ConA), conjugated to Alexa Fluor 488, and further analyzed by flow cytometry. Our results demonstrated that more than 98% of the vesicles were recognized by this lectin, confirming the presence of mannosylated proteins on EV surface **(Fig. 6)**. Strikingly, EVs obtained from the acapsular *cap59Δ* mutant strain also showed a high percentage of staining (94.3%), which suggested that mannoproteins could essentially be the outer vesicle decoration.

bioRxiv preprint doi: https://doi.org/10.1101/2020.08.17.253716; this version posted August 17, 2020. The copyright holder for this preprint (which was not certified by peer review) is the author/funder, who has granted bioRxiv a license to display the preprint in perpetuity. It is made available under aCC-BY-NC-ND 4.0 International license.

Two of the most abundant *C. neoformans* EV-associated proteins (Mp88) and Vep1/CNAG_03223) are both GPI-anchored and represent 23.7% of the total identified proteins in the EV extract. Indeed, in all three species, Mp88 (Huang et al. 2002) was the most prevalent protein. In *C. deuterogatii* EVs, in which the Vep1 protein is not present, Mp88 represents 35.4% of the total amount of protein present in the EV extract. We constructed the corresponding single mutant strains for *mp88*Δ and *vep1*Δ, and tested for ConA binding. However, EVs purified from both single mutants showed similar ConA binding percentages to wild type EVs (data not shown), suggesting that cryptococcal EVs might bear a highly complex decoration, probably formed from a dynamic combination of mannoproteins.

Combining all these data, we propose a model for cryptococcal EV structure, in which, EVs are decorated by mannosylated proteins and covered by GXM **(Fig. 7)**.

- ***EVs for immunization and protection against cryptococcal infection***

Proteomic analysis of the *C. neoformans* EVs identified many immunogenic proteins, including Mp88, the members of Gox and Cda families and some Vep proteins previously tested as vaccine candidates against cryptococcosis (Specht et al. 2017, Hester et al. 2020). Moreover, some of these proteins were also found to be enriched in *C. deneoformans* and *C. deuterogattii* EVs (Mp88, Cda1, Cda2, Cda3, and Gox2), suggesting that secretion of these immunogenic molecules via EVs could be a conserved feature across different species.

Taking into account that cryptococcal EVs have been shown to be immune modulators (Freitas et al. 2019) and may impact the pathophysiology of the infection (Bielska et al. 2018, Hai et al. 2020), we reasoned that EVs could be used as vaccines against cryptococcosis avoiding the need for recombinant protein purification and adjuvant usage. The usage of fungal EVs has been previously suggested as a promising vaccine strategy (Vargas et al. 2015, Colombo et al. 2019, Freitas et al. 2019, Vargas et al. 2020). However, cryptococcal EVs have never been tested in murine infection mode so far.

As a pilot experiment, we first purified EVs from *C. neoformans* WT strain and from the acapsular *cap59*Δ strain, and used them to immunize BALB/c mice in two different EV-protein extracts dosages (1 and 10 µg) via intraperitoneal injections; each group, including the control group, contained four mice. After three immunizations, the anti-EV-antibody response in the mice was evaluated. Regardless of EV origin, all the immunized mice produced antibodies against vesicular molecules, as revealed by Western Blot assay **(Fig. 8A)**. Forty days after the last immunization, mice were challenged intranasally with 10^4 *C. neoformans* strain KN99α cells, and their survival were monitored post-infection. All EV-immunized mice

bioRxiv preprint doi: https://doi.org/10.1101/2020.08.17.253716; this version posted August 17, 2020. The copyright holder for this preprint (which was not certified by peer review) is the author/funder, who has granted bioRxiv a license to display the preprint in perpetuity. It is made available under aCC-BY-NC-ND 4.0 International license.

survived longer than the non-immunized ones and, immunization with both doses of *cap59*Δ EVs prolonged mice survival in a statistically significant way **(Fig. 8B)** To note, the total carbohydrate per 100 µg of EV-proteins were approximately 22 µg and 3 µg, respectively, for the WT and *cap59*Δ mutant, as analyzed by gas-chromatography analyses (Richie et al. 2009).

We then confirmed this result using a larger number of mice (10 mice per group). Since the highest dose of EVs from the acapsular mutant rendered the best protection, we decided to proceed only with EVs from *cap59*Δ strain (10 µg). After repeated immunizations with EVs, the mice anti-EV-antibody response was analyzed; all immunized mice produced antibodies against vesicular molecules **(Fig. 8C)**. Following, the mice were challenged with 10^4 *C. neoformans* strain KN99α cells, and their survival was monitored post-infection. The EV-based immunization rendered a significant prolonged survival (p=0.0006) **(Fig. 8D)**, thus confirming the promising potential usage of EV-based protection against *Cryptococcus*.

4. Discussion

Studies on fungal EVs have gained much attention during the last years (Rizzo et al. 2020). Although many promising data coming from pathogenic and nonpathogenic species highlight their importance in diverse biological contexts, knowledge on fungal EVs is still limited, mostly due to their nanometer size and the technical hurdles intrinsic to the methods applied for their characterization (Rizzo et al. 2020). We here used cutting edge technologies to revisit *Cryptococcus* EVs. Our cryo-EM analysis showed an unprecedented quality of EV images and resolved the fibrillar structure decoration as a new aspect on fungal EVs.

Our hypothesis is that EV decoration is made of mannoproteins. This is supported by two independent experiments. First, we demonstrated that although GXM most probably surrounds the vesicles, it is not necessary for the presence of decoration. Thus, EVs produced by an acapsular strains are not bound by a GXM specific antibody yet, they displayed the type of decoration and, in a similar percentage of EVs. Secondly, *C. albicans* and *S. cerevisiae* EVs are also decorated, although none of these strains produced a polysaccharide capsule. Nonetheless, our results revealed that the deletion of single mannoproteins, such as the GPI-anchored proteins Mp88 and Vep1, was not sufficient to completely remove the EV decoration, suggesting that this structure has a highly complex and dynamic composition, including several mannoproteins. Indeed, previous reports in *C. albicans* showed that the role of GPI-anchored proteins are redundant and single mutants mostly displayed minor phenotypes, if any (Plaine et al. 2008).

bioRxiv preprint doi: https://doi.org/10.1101/2020.08.17.253716; this version posted August 17, 2020. The copyright holder for this preprint (which was not certified by peer review) is the author/funder, who has granted bioRxiv a license to display the preprint in perpetuity. It is made available under aCC-BY-NC-ND 4.0 International license.

Interestingly, in 2018 Johansson and colleagues performed cryo-EM analysis of *Malassezia sympodialis* EVs demonstrating no decoration on their surface (Johansson et al. 2018). Comparative genomic analysis suggested that this lipophilic pathogenic yeast, living on the skin (Theelen et al. 2018), lacks the N-glycosylation pathway and possesses only a very small number of GPI-anchor proteins (Gioti et al. 2013). Accordingly, *M. sympodialis* cells lack the extensive mannan outer fibrillar layer, which can be easily observed at the surface of the cell wall of most yeasts including *S. cerevisiae* or *C. albicans* (Gioti et al. 2013, Muszewska et al. 2017). Therefore, it is very tempting to hypothesize that this absence of mannans in *M. sympodialis* could explain the absence of EV decoration, supporting the idea that these are mannoprotein-based.

Previous proteomic analysis of fungal EVs identified putative mannoproteins, suggesting that this decoration is a common feature of fungal EVs (Bleackley et al. 2019, Dawson et al. 2020, Karkowska-Kuleta et al. 2020, Rizzo et al. 2020). Accordingly, it was recently shown that *C. glabrata* EVs bound by the ConA lectin in flow cytometry experiments (Karkowska-Kuleta et al. 2020) and that *Aspergillus fumigatus* protoplasts, when submitted to cell wall regeneration, also release EVs which seem to be covered by fibril-like structures (Rizzo et al. 2020).

Whereas the presence of decoration seems to be a hallmark of fungal EV, they are not specific to this kingdom. Although EVs bearing visible structures on their surface have not been commonly reported, a recent cryo-EM analysis of EVs derived from human breast cell lines overexpressing hyaluronan synthase 3-(HAS3) recently suggested the presence of fibril-like structures on the vesicle surface (Noble et al. 2020). Additionally, EVs from poliovirus-infected cells contain 'protein structures with globular heads on a stalk' around the membrane (Yang et al. 2020). Nevertheless, it is still unclear how often this feature is present among the whole EV population, and what the composition of these surface structures is.

Previous reports explored the size and morphology of fungal EV populations, mostly by techniques comprising electron microscopy (TEM, SEM), dynamic light scattering (DLS), and NTA (Albuquerque et al. 2008, Rodrigues et al. 2008, Wolf et al. 2014, Vargas et al. 2015, Wolf et al. 2015, Bielska and May 2019). Here we show that cryptococcal EVs are much more heterogeneous than showed before, comprising not only the regular EVs but also tubular, flat, and multilayered EVs. This description is reasonably different from the conventional view that EVs are only based on double-membrane spherical structures. Although the different EV morphologies were previously identified in many fungal pathogens (Albuquerque et al. 2008, Rodrigues et al. 2008, Tefsen et al. 2014, Vargas et al. 2015), some vesicular shapes found in

bioRxiv preprint doi: https://doi.org/10.1101/2020.08.17.253716; this version posted August 17, 2020. The copyright holder for this preprint (which was not certified by peer review) is the author/funder, who has granted bioRxiv a license to display the preprint in perpetuity. It is made available under aCC-BY-NC-ND 4.0 International license.

this work were not commonly observed in previous EVs analysis, such as tubular and flat structures, and their relative proportions no evaluated.

Membrane tubule structures (memtubs) budding from the plasma membrane were found in the arbuscular fungus *Rhizophagus irregularis*, suggesting that different shapes of membranous structures could appear during fungal growth (Roth et al. 2019). Additionally, tubular and other morphologies were also found in EV populations obtained from human biological fluids (Arraud et al. 2014, Emelyanov et al. 2020). Although these data suggest that diverse structures could be part of the native EV population, the cellular origins of these structures are still unknown, and we cannot rule out the possibility of being artifacts resulted from the filtration step of the commonly used EV isolation protocols.

In this study, we demonstrated that *C. neoformans* releases both decorated and undecorated EVs adding another previously unappreciated aspect on fungal EV diversity. As hypothesized before, this result also suggests the existence of two different pathways involved in EV biogenesis (Oliveira et al. 2010, Oliveira et al. 2013, Bielska and May 2019, Rizzo et al. 2020). It is, therefore, reasonable to hypothesize that decorated EVs could have shed out from the fungal plasma membrane, "stealing" cell membrane proteins when they bud out. Interestingly, the decorated EVs are usually larger than the undecorated ones, which is in good adequacy with what would be typical microvesicles in mammals. In this hypothesis, the enrichment of tetraspanin membrane proteins containing a SUR7/PalI family motif might indicate that decorated EVs could be specifically shed from the Sur7 specialized plasma membrane domains. This model could be extended to other fungi as Sur7 proteins have been recently identified as EV- protein markers in *C. albicans* and in the wheat pathogen *Zymoseptoria tritici* (Dawson et al. 2020, Hill and Solomon 2020). This latter hypothesis, together with whether or not the smaller undecorated EVs are a result of the endosomal secretory pathways, considered as exosomes being released by multivesicular bodies (MVB), still needs to be further explored. Interestingly, the characterization of decorated and undecorated EVs as microvesicles and exosomes, respectively, were previously assumed (Noble et al. 2020). This hypothesis and our current results are supported by a recent study of *A. fumigatus* EVs in the absence of a cell wall. EVs were clearly formed at the plasma membrane level and they contained a number of plasma membrane proteins (Rizzo et al. 2020).

Our work suggests that fungal EV cargo contains proteins involved in diverse biological processes, including Mp88 and members of Cda and Gox families, which have been suggested as immunomodulators (Specht et al. 2017, Hester et al. 2020). Since the novel surface structure on fungal EV resolved by cryo-EM resembles the spike complexes on viral envelopes (Neuman

bioRxiv preprint doi: https://doi.org/10.1101/2020.08.17.253716; this version posted August 17, 2020. The copyright holder for this preprint (which was not certified by peer review) is the author/funder, who has granted bioRxiv a license to display the preprint in perpetuity. It is made available under aCC-BY-NC-ND 4.0 International license.

et al. 2006, Zanetti et al. 2006), we reasoned their use as a vaccine platform approach. Numerous efforts have been carried out in developing vaccines against fungal infections. Some of these challenges engaged in different stages of clinical trials; however, none of them could be finally approved for public use (Nami et al. 2019). It was previously shown that the pre-treatment of *Galleria mellonella* larvae with fungal EVs stimulated a protective response against a lethal challenge with *C. albicans* or C. *neoformans* (Vargas et al. 2015, Colombo et al. 2019). More recently, it was also demonstrated that *C. albicans* EVs were also able to elicit a protective effect against murine candidiasis (Vargas et al. 2020). Interestingly, *C. neoformans* EV have shown to be immune reactive with sera from patients with cryptococcosis, indicating that EV-associated proteins are produced during cryptococcal infection and that they might be used as vaccines (Rodrigues et al. 2008). Prophylactic immunization is one of the effective methods to prevent cryptococcal infection, and several cryptococcal antigens have been tested for their vaccination potential (Caballero Van Dyke and Wormley 2018, Ueno et al. 2020). However, the *in vivo* immunoregulatory role of EVs have largely remained unknown (Robbins and Morelli 2014).

In our study, antibody responses in cryptococcal EV-immunized mice indicate that the EVs are capable of eliciting an adaptive immune response in the absence of any adjuvants or carriers, unlike other antigenic proteins of *Cryptococcus* (Specht et al. 2017). EV-based vaccination data obtained by other groups using an invertebrate model suggest that innate immunity might also be involved (Vargas et al. 2015, Colombo et al. 2019). As *Cryptococcus* predominantly infects immunocompromised hosts, it will be worth checking the role of EVs in eliciting trained immunity, wherein innate immune cells develop memory-like response against an antigen upon repeated exposure (Hole et al. 2019, Mulder et al. 2019). The mechanisms, and the responsible immune cell types leading to prolonged survival in our murine infection model remain thus to be identified. Although EVs immunizations were not sufficient to prevent the animal death, we believe that adjusting the antigens exposed on EV surface could potentially increase the protective effect. In that sense, the fact EV from *C. neoformans* WT strain showed a reduced effect on mice survival, compared to EVs obtained from the acapsular mutant, which is a very encouraging data.

Overall, the fantastic power of cryo-EM, together with a number of innovative analyses, allowed us to draw a new model of fungal EVs and revealed new aspects of their diversity, suggesting different biosynthetic pathways. This model supports new strategies to construct vaccines against these still too often neglected infectious diseases. It also opens the door to more questions concerning the origin and the fate of the fungal EVs.

bioRxiv preprint doi: https://doi.org/10.1101/2020.08.17.253716; this version posted August 17, 2020. The copyright holder for this preprint (which was not certified by peer review) is the author/funder, who has granted bioRxiv a license to display the preprint in perpetuity. It is made available under aCC-BY-NC-ND 4.0 International license.

5. References

Albuquerque PC, Nakayasu ES, Rodrigues ML, Frases S, Casadevall A, Zancope-Oliveira RM, Almeida IC, Nosanchuk JD 2008. Vesicular transport in *Histoplasma capsulatum:* an effective mechanism for trans-cell wall transfer of proteins and lipids in ascomycetes. *Cell Microbiol* 10: 1695-1710.

Almagro Armenteros JJ, Tsirigos KD, Sønderby CK, Petersen TN, Winther O, Brunak S, von Heijne G, Nielsen H 2019. SignalP 5.0 improves signal peptide predictions using deep neural networks. *Nature Biotechnology* 37: 420-423.

Arraud N, Linares R, Tan S, Gounou C, Pasquet JM, Mornet S, Brisson AR 2014. Extracellular vesicles from blood plasma: determination of their morphology, size, phenotype and concentration. *Journal of Thrombosis and Haemostasis* 12: 614-627.

Bachurski D, Schuldner M, Nguyen P-H, Malz A, Reiners KS, Grenzi PC, Babatz F, Schauss AC, Hansen HP, et al. 2019. Extracellular vesicle measurements with nanoparticle tracking analysis - An accuracy and repeatability comparison between NanoSight NS300 and ZetaView. *Journal of extracellular vesicles* 8: 1596016-1596016.

Baker LG, Specht CA, Lodge JK 2011. Cell Wall Chitosan Is Necessary for Virulence in the Opportunistic Pathogen *Cryptococcus neoformans*. *Eukaryot Cell* 10: 1264.

Bielska E, May RC 2019. Extracellular vesicles of human pathogenic fungi. *Curr Opinion Microbiol* 52: 90-99.

Bielska E, Sisquella MA, Aldeieg M, Birch C, O'Donoghue EJ, May RC 2018. Pathogen-derived extracellular vesicles mediate virulence in the fatal human pathogen Cryptococcus gattii. *Nature communications* 9: 1556-1556.

Bleackley MR, Dawson CS, Anderson MA 2019. Fungal Extracellular Vesicles with a Focus on Proteomic Analysis. *PROTEOMICS* 19: 1800232.

Bleackley MR, Samuel M, Garcia-Ceron D, McKenna JA, Lowe RGT, Pathan M, Zhao K, Ang C-S, Mathivanan S, et al. 2020. Extracellular Vesicles From the Cotton Pathogen Fusarium oxysporum f. sp. vasinfectum Induce a Phytotoxic Response in Plants. *Frontiers in plant science* 10: 1610-1610.

Caballero Van Dyke MC, Wormley FL, Jr. 2018. A Call to Arms: Quest for a Cryptococcal Vaccine. *Trends Microbiol* 26: 436-446.

Casadevall A, Mukherjee J, Devi SJN, Schneerson R, Robbins JB, Scharff MD 1992. Antibodies Elicited by a Cryptococcus neoformans-Tetanus Toxoid Conjugate Vaccine Have the Same Specificity as Those Elicited in Infection. *The Journal of Infectious Diseases* 165: 1086-1093.

Chiang C-Y, Chen C 2019. Toward characterizing extracellular vesicles at a single-particle level. *J Biomed Sci* 26: 9-9.

Chiou N-T, Kageyama R, Ansel KM 2018. Selective Export into Extracellular Vesicles and Function of tRNA Fragments during T Cell Activation. *Cell Rep.* 25: 3356-3370.e3354.

Chun CD, Brown JCS, Madhani HD 2011. A major role for capsule-independent phagocytosis-inhibitory mechanisms in mammalian infection by Cryptococcus neoformans. *Cell host & microbe* 9: 243-251.

Coakley G, McCaskill JL, Borger JG, Simbari F, Robertson E, Millar M, Harcus Y, McSorley HJ, Maizels RM, et al. 2017. Extracellular Vesicles from a Helminth Parasite Suppress Macrophage Activation and Constitute an Effective Vaccine for Protective Immunity. *Cell Rep.* 19: 1545-1557.

Collopy PD, Colot HV, Park G, Ringelberg C, Crew CM, Borkovich KA, Dunlap JC 2010. High-throughput construction of gene deletion cassettes for generation of *Neurospora crassa* knockout strains. *Methods Mol Biol* 638: 33-40.

Colombo AC, Rella A, Normile T, Joffe LS, Tavares PM, de S. Araújo GR, Frases S, Orner EP, Farnoud AM, et al. 2019. Cryptococcus neoformans Glucuronoxylomannan and Sterylglucoside Are Required for Host Protection in an Animal Vaccination Model. *mBio* 10: e02909-02918.

Cox J, Mann M 2008. MaxQuant enables high peptide identification rates, individualized p.p.b.-range mass accuracies and proteome-wide protein quantification. *Nature Biotechnology* 26: 1367-1372.

bioRxiv preprint doi: https://doi.org/10.1101/2020.08.17.253716; this version posted August 17, 2020. The copyright holder for this preprint (which was not certified by peer review) is the author/funder, who has granted bioRxiv a license to display the preprint in perpetuity. It is made available under aCC-BY-NC-ND 4.0 International license.

Cox J, Neuhauser N, Michalski A, Scheltema RA, Olsen JV, Mann M 2011. Andromeda: A Peptide Search Engine Integrated into the MaxQuant Environment. *Journal of Proteome Research* 10: 1794-1805.

da Silva RP, Puccia R, Rodrigues ML, Oliveira DL, Joffe LS, César GV, Nimrichter L, Goldenberg S, Alves LR 2015. Extracellular vesicle-mediated export of fungal RNA. *Sci. Rep.* 5: 7763.

Dawson CS, Garcia-Ceron D, Rajapaksha H, Faou P, Bleackley MR, Anderson MA 2020. Protein markers for Candida albicans EVs include claudin-like Sur7 family proteins. *Journal of Extracellular Vesicles* 9: 1750810.

de Groot PWJ, Hellingwerf KJ, Klis FM 2003. Genome-wide identification of fungal GPI proteins. *Yeast* 20: 781-796.

Deatherage BL, Cookson BT 2012. Membrane Vesicle Release in Bacteria, Eukaryotes, and Archaea: a Conserved yet Underappreciated Aspect of Microbial Life. *Infect Immun* 80: 1948.

Eisenman HC, Frases S, Nicola AM, Rodrigues ML, Casadevall A 2009. Vesicle-associated melanization in Cryptococcus neoformans. *Microbiology* 155: 3860-3867.

Emelyanov A, Shtam T, Kamyshinsky R, Garaeva L, Verlov N, Miliukhina I, Kudrevatykh A, Gavrilov G, Zabrodskaya Y, et al. 2020. Cryo-electron microscopy of extracellular vesicles from cerebrospinal fluid. *PLOS ONE* 15: e0227949.

Fan Y, Lin X 2018. Multiple Applications of a Transient CRISPR-Cas9 Coupled with Electroporation (TRACE) System in the *Cryptococcus neoformans* Species Complex. *Genetics* 208: 1357.

Ferrareze PAG, Maufrais C, Silva Araujo Streit R, Priest S, Cuomo C, Heitman J, Staats CC, Janbon G 2020. A validate pipeline for annotation of complex fungal genomes: application to *Cryptococcus deuterogatii* genome annotation *submitted*.

Freitas MS, Bonato VLD, Pessoni AM, Rodrigues ML, Casadevall A, Almeida F 2019. Fungal Extracellular Vesicles as Potential Targets for Immune Interventions. *mSphere* 4: e00747-00719.

Gioti A, Nystedt B, Li W, Xu J, Andersson A, Averette AF, Münch K, Wang X, Kappauf C, et al. 2013. Genomic Insights into the Atopic Eczema-Associated Skin Commensal Yeast <em>Malassezia sympodialis</em&gt. *mBio* 4: e00572-00512.

Hai TP, Tuan TL, Van Anh D, Mai TN, Phu Huong LN, Thwaites GE, Johnson E, Van Vinh Chau N, Ashton P, et al. 2020. The expression of virulence by the Cryptococcus neoformans VNIa-5 lineage is plastic and associated with host immune background. *bioRxiv*: 2020.2002.2024.962134.

Hester MM, Lee CK, Abraham A, Khoshkenar P, Ostroff GR, Levitz SM, Specht CA 2020. Protection of mice against experimental cryptococcosis using glucan particle-based vaccines containing novel recombinant antigens. *Vaccine* 38: 620-626.

Hill E, Solomon P (2020). Extracellular Vesicles from the Apoplastic Fungal Wheat Pathogen Zymoseptoria Tritici, Research Square.

Hole CR, Wager CML, Castro-Lopez N, Campuzano A, Cai H, Wozniak KL, Wang Y, Wormley FL 2019. Induction of memory-like dendritic cell responses in vivo. *Nature Communications* 10: 2955.

Huang C, Nong SH, Mansour MK, Specht CA, Levitz SM 2002. Purification and characterization of a second immunoreactive mannoprotein from *Cryptococcus neoformans* that stimulates T-cell responses. *Infect Immun* 70: 5485-5493.

Joffe LS, Nimrichter L, Rodrigues ML, Del Poeta M 2016. Potential Roles of Fungal Extracellular Vesicles during Infection. *mSphere* 1: e00099-00016.

Johansson HJ, Vallhov H, Holm T, Gehrmann U, Andersson A, Johansson C, Blom H, Carroni M, Lehtiö J, et al. 2018. Extracellular nanovesicles released from the commensal yeast Malassezia sympodialis are enriched in allergens and interact with cells in human skin. *Sci. Rep.* 8: 9182.

Jung WH, Sham A, Lian T, Singh A, Kosman DJ, Kronstad JW 2008. Iron Source Preference and Regulation of Iron Uptake in Cryptococcus neoformans. *PLoS Pathog* 4: e45.

Karkowska-Kuleta J, Kulig K, Karnas E, Zuba-Surma E, Woznicka O, Pyza E, Kuleta P, Osyczka A, Rapala-Kozik M, et al. 2020. Characteristics of extracellular vesicles released by the pathogenic yeast-like fungi *Candida glabrata*, *Candida parapsilosis* and *Candida tropicalis*. *Cells* 9: 1722.

Kremer JR, Mastronarde DN, McIntosh JR 1996. Computer Visualization of Three-Dimensional Image Data Using IMOD. *Journal of Structural Biology* 116: 71-76.

bioRxiv preprint doi: https://doi.org/10.1101/2020.08.17.253716; this version posted August 17, 2020. The copyright holder for this preprint (which was not certified by peer review) is the author/funder, who has granted bioRxiv a license to display the preprint in perpetuity. It is made available under aCC-BY-NC-ND 4.0 International license.

Krogh A, Larsson B, von Heijne G, Sonnhammer ELL 2001. Predicting transmembrane protein topology with a hidden markov model: application to complete genomes. *J Mol Biol* 305: 567-580.

Leone F, Bellani L, Muccifora S, Giorgetti L, Bongioanni P, Simili M, Maserti B, Del Carratore R 2018. Analysis of extracellular vesicles produced in the biofilm by the dimorphic yeast Pichia fermentans. *Journal of Cellular Physiology* 233: 2759-2767.

Levitz SM, Nong S, Mansour MK, Huang C, Specht CA 2001. Molecular characterization of a mannoprotein with homology to chitin deacetylases that stimulates T cell responses to Cryptococcus neoformans. *Proc Natl Acad Sci USA* 98: 10422-10427.

Maas SLN, de Vrij J, van der Vlist EJ, Geragousian B, van Bloois L, Mastrobattista E, Schiffelers RM, Wauben MHM, Broekman MLD, et al. 2015. Possibilities and limitations of current technologies for quantification of biological extracellular vesicles and synthetic mimics. *Journal of Controlled Release* 200: 87-96.

Mastronarde DN 2005. Automated electron microscope tomography using robust prediction of specimen movements. *Journal of Structural Biology* 152: 36-51.

Mastronarde DN, Held SR 2017. Automated tilt series alignment and tomographic reconstruction in IMOD. *Journal of structural biology* 197: 102-113.

Meldolesi J 2018. Exosomes and Ectosomes in Intercellular Communication. *Curr Biol* 28: R435-R444.

Moyrand F, Fontaine T, Janbon G 2007. Systematic capsule gene disruption reveals the central role of galactose metabolism on *Cryptococcus neoformans* virulence. *Mol Microbiol* 64: 771-781.

Mulder WJM, Ochando J, Joosten LAB, Fayad ZA, Netea MG 2019. Therapeutic targeting of trained immunity. *Nat Rev Drug Discov* 18: 553-566.

Muszewska A, Piłsyk S, Perlińska-Lenart U, Kruszewska JS 2017. Diversity of Cell Wall Related Proteins in Human Pathogenic Fungi. *Journal of fungi (Basel, Switzerland)* 4: 6.

Nami S, Mohammadi R, Vakili M, Khezripour K, Mirzaei H, Morovati H 2019. Fungal vaccines, mechanism of actions and immunology: A comprehensive review. *Biomedicine & Pharmacotherapy* 109: 333-344.

Neuman BW, Adair BD, Yoshioka C, Quispe JD, Orca G, Kuhn P, Milligan RA, Yeager M, Buchmeier MJ 2006. Supramolecular architecture of severe acute respiratory syndrome coronavirus revealed by electron cryomicroscopy. *J Virol* 80: 7918-7928.

Noble JM, Roberts LM, Vidavsky N, Chiou AE, Fischbach C, Paszek MJ, Estroff LA, Kourkoutis LF 2020. Direct comparison of optical and electron microscopy methods for structural characterization of extracellular vesicles. *Journal of Structural Biology* 210: 107474.

O'Meara TR, Alspaugh JA 2012. The Cryptococcus neoformans capsule: a sword and a shield. *Clin Microbiol Rev* 25: 387-408.

Oliveira DL, Freire-de-Lima CG, Nosanchuk JD, Casadevall A, Rodrigues ML, Nimrichter L 2010. Extracellular vesicles from *Cryptococcus neoformans* modulate macrophage functions. *Infect Immun* 78: 1601-1609.

Oliveira DL, Nakayasu ES, Joffe LS, Guimarães AJ, Sobreira TJP, Nosanchuk JD, Cordero RJB, Frases S, Casadevall A, et al. 2010. Characterization of Yeast Extracellular Vesicles: Evidence for the Participation of Different Pathways of Cellular Traffic in Vesicle Biogenesis. *PLOS ONE* 5: e11113.

Oliveira DL, Nimrichter L, Miranda K, Frases S, Faull KF, Casadevall A, Rodrigues ML 2009. Cryptococcus neoformans cryoultramicrotomy and vesicle fractionation reveals an intimate association between membrane lipids and glucuronoxylomannan. *Fungal Genet Biol* 46: 956-963.

Oliveira DL, Rizzo J, Joffe LS, Godinho RMC, Rodrigues ML 2013. Where do they come from and where do they go: candidates for regulating extracellular vesicle formation in fungi. *Int J Mol Sci* 14: 9581-9603.

Orlov I, Myasnikov AG, Andronov L, Natchiar SK, Khatter H, Beinsteiner B, Ménétret J-F, Hazemann I, Mohideen K, et al. 2017. The integrative role of cryo electron microscopy in molecular and cellular structural biology. *Biology of the Cell* 109: 81-93.

Pettersen EF, Goddard TD, Huang CC, Couch GS, Greenblatt DM, Meng EC, Ferrin TE 2004. UCSF Chimera—A visualization system for exploratory research and analysis. *Journal of Computational Chemistry* 25: 1605-1612.

bioRxiv preprint doi: https://doi.org/10.1101/2020.08.17.253716; this version posted August 17, 2020. The copyright holder for this preprint (which was not certified by peer review) is the author/funder, who has granted bioRxiv a license to display the preprint in perpetuity. It is made available under aCC-BY-NC-ND 4.0 International license.

Pierleoni A, Martelli PL, Casadio R 2008. PredGPI: a GPI-anchor predictor. *BMC Bioinformatics* 9: 392.

Plaine A, Walker L, Da Costa G, Mora-Montes HM, McKinnon A, Gow NAR, Gaillardin C, Munro CA, Richard ML 2008. Functional analysis of Candida albicans GPI-anchored proteins: roles in cell wall integrity and caspofungin sensitivity. *Fungal genetics and biology : FG & B* 45: 1404-1414.

Rajasingham R, Smith RM, Park BJ, Jarvis JN, Govender NP, Chiller TM, Denning DW, Loyse A, Boulware DR 2017. Global burden of disease of HIV-associated cryptococcal meningitis: an updated analysis. *The Lancet Infectious Diseases* 17: 873-881.

Rayner S, Bruhn S, Vallhov H, Andersson A, Billmyre RB, Scheynius A 2017. Identification of small RNAs in extracellular vesicles from the commensal yeast Malassezia sympodialis. *Sci. Rep.* 7: 39742.

Reis FCG, Borges BS, Jozefowicz LJ, Sena BAG, Garcia AWA, Medeiros LC, Martins ST, Honorato L, Schrank A, et al. 2019. A Novel Protocol for the Isolation of Fungal Extracellular Vesicles Reveals the Participation of a Putative Scramblase in Polysaccharide Export and Capsule Construction in Cryptococcus gattii. *mSphere* 4: e00080-00019.

Richie DL, Hartl L, Aimanianda V, Winters MS, Fuller KK, Miley MD, White S, McCarthy JW, Latgé J-P, et al. 2009. A role for the unfolded protein response (UPR) in virulence and antifungal susceptibility in Aspergillus fumigatus. *PLoS Pathog* 5: e1000258-e1000258.

Rizzo J, Albuquerque PC, Wolf JM, Nascimento R, Pereira MD, Nosanchuk JD, Rodrigues ML 2017. Analysis of multiple components involved in the interaction between Cryptococcus neoformans and Acanthamoeba castellanii. *Fungal Biology* 121: 602-614.

Rizzo J, Chaze T, Miranda K, Roberson RW, Gorgette O, Nimrichter L, Matondo M, Latgé J-P, Beauvais A, et al. 2020. Characterization of extracellular vesicles produced by *Aspergillus fumigatus* protoplasts. *mSphere* 5: e00476-00420.

Rizzo J, Rodrigues ML, Janbon G 2020. Extracellular Vesicles in Fungi: Past, Present, and Future Perspectives. *Frontiers in Cellular and Infection Microbiology* 10.

Robbins PD, Morelli AE 2014. Regulation of immune responses by extracellular vesicles. *Nat Rev Immunol* 14: 195-208.

Rodrigues ML, Casadevall A 2018. A two-way road: novel roles for fungal extracellular vesicles. *Mol Microbiol* 110: 11-15.

Rodrigues ML, Godinho RMC, Zamith-Miranda D, Nimrichter L 2015. Traveling into Outer Space: Unanswered Questions about Fungal Extracellular Vesicles. *PLoS Pathog* 11: e1005240.

Rodrigues ML, Nakayasu ES, Oliveira DL, Nimrichter L, Nosanchuk JD, Almeida IC, A. C 2008. Extracellular vesicles produced by *Cryptococcus neoformans* contain protein components associated with virulence. *Eukaryot Cell* 7: 58-67.

Rodrigues ML, Nimrichter L, Oliveira DL, Frases S, Miranda K, Zaragoza O, Alvarez M, Nakouzi A, Feldmesser M, et al. 2007. Vesicular polysaccharide export in *Cryptococcus neoformans* is a eukaryotic solution to the problem of fungal trans-cell wall transport. *Eukaryot Cell* 6: 48-59.

Roth R, Hillmer S, Funaya C, Chiapello M, Schumacher K, Lo Presti L, Kahmann R, Paszkowski U 2019. Arbuscular cell invasion coincides with extracellular vesicles and membrane tubules. *Nature Plants* 5: 204-211.

Schorb M, Haberbosch I, Hagen WJH, Schwab Y, Mastronarde DN 2019. Software tools for automated transmission electron microscopy. *Nature Meth* 16: 471-477.

Schwanhäusser B, Busse D, Li N, Dittmar G, Schuchhardt J, Wolf J, Chen W, Selbach M 2011. Global quantification of mammalian gene expression control. *Nature* 473: 337-342.

Shopova IA, Belyaev I, Dasari P, Jahreis S, Stroe MC, Cseresnyés Z, Zimmermann A-K, Medyukhina A, Svensson C-M, et al. 2020. Human Neutrophils Produce Antifungal Extracellular Vesicles against *Aspergillus fumigatus*. *mBio* 11: e00596-00520.

Souza JAM, Baltazar LdM, Carregal VM, Gouveia-Eufrasio L, de Oliveira AG, Dias WG, Campos Rocha M, Rocha de Miranda K, Malavazi I, et al. 2019. Characterization of *Aspergillus fumigatus* extracellular vesicles and their effects on macrophages and neutrophils functions. *Frontiers in microbiology* 10: 2008-2008.

Specht CA, Lee CK, Huang H, Hester MM, Liu J, Luckie BA, Torres Santana MA, Mirza Z, Khoshkenar P, et al. 2017. Vaccination with Recombinant Cryptococcus Proteins in Glucan Particles Protects Mice

bioRxiv preprint doi: https://doi.org/10.1101/2020.08.17.253716; this version posted August 17, 2020. The copyright holder for this preprint (which was not certified by peer review) is the author/funder, who has granted bioRxiv a license to display the preprint in perpetuity. It is made available under aCC-BY-NC-ND 4.0 International license.

against Cryptococcosis in a Manner Dependent upon Mouse Strain and Cryptococcal Species. *mBio* 8: e01872-01817.

Tefsen B, Grijpstra J, Ordonez S, Lammers M, van Die I, de Cock H 2014. Deletion of the CAP10 gene of Cryptococcus neoformans results in a pleiotropic phenotype with changes in expression of virulence factors. *Research in Microbiology* 165: 399-410.

Theelen B, Cafarchia C, Gaitanis G, Bassukas ID, Boekhout T, Dawson TL, Jr. 2018. Malassezia ecology, pathophysiology, and treatment. *Med Mycol* 56: S10-S25.

Théry C, Witwer KW, Aikawa E, Alcaraz MJ, Anderson JD, Andriantsitohaina R, Antoniou A, Arab T, Archer F, et al. 2018. Minimal information for studies of extracellular vesicles 2018 (MISEV2018): a position statement of the International Society for Extracellular Vesicles and update of the MISEV2014 guidelines. *Journal of extracellular vesicles* 7: 1535750-1535750.

Tyanova S, Temu T, Cox J 2016. The MaxQuant computational platform for mass spectrometry-based shotgun proteomics. *Nature Protocols* 11: 2301-2319.

Ueno K, Yanagihara N, Shimizu K, Miyazaki Y 2020. Vaccines and protective immune memory against Cryptococcosis. *Biol. Pharm. Bull.* 43.

Vallejo MC, Nakayasu ES, Longo LVG, Ganiko L, Lopes FG, Matsuo AL, Almeida IC, Puccia R 2012. Lipidomic analysis of extracellular vesicles from the pathogenic phase of Paracoccidioides brasiliensis. *PloS one* 7: e39463-e39463.

Van Der Pol E, Hoekstra AG, Sturk A, Otto C, Van Leeuwen TG, Nieuwland R 2010. Optical and non-optical methods for detection and characterization of microparticles and exosomes. *Journal of Thrombosis and Haemostasis* 8: 2596-2607.

van Niel G, D'Angelo G, Raposo G 2018. Shedding light on the cell biology of extracellular vesicles. *Nature Reviews Molecular Cell Biology* 19: 213-228.

Vargas G, Honorato L, Guimarães AJ, Rodrigues ML, Reis FCG, Vale AM, Ray A, Nosanchuk JD, Nimrichter L 2020. Protective effect of fungal extracellular vesicles against murine candidiasis. *Cell Microbiol* n/a: e13238.

Vargas G, Rocha JDB, Oliveira DL, Albuquerque PC, Frases S, Santos SS, Nosanchuk JD, Gomes AMO, Medeiros LCAS, et al. 2015. Compositional and immunobiological analyses of extracellular vesicles released by Candida albicans. *Cell Microbiol* 17: 389-407.

Wallace EWJ, Maufrais C, Sales-Lee J, Tuck LR, de Oliveira L, Feuerbach F, Moyrand F, Natarajan P, Madhani HD, et al. 2020. Quantitative global studies reveal differential translational control by start codon context across the fungal kingdom. *Nucleic Acids Res.* 48: 2312-2331.

Wang X, Thompson CD, Weidenmaier C, Lee JC 2018. Release of Staphylococcus aureus extracellular vesicles and their application as a vaccine platform. *Nature communications* 9: 1379-1379.

Witwer KW, Théry C 2019. Extracellular vesicles or exosomes? On primacy, precision, and popularity influencing a choice of nomenclature. *Journal of Extracellular Vesicles* 8: 1648167.

Wolf JM, Espadas-Moreno J, Luque-Garcia JL, Casadevall A 2014. Interaction of *Cryptococcus neoformans* extracellular vesicles with the cell wall. *Eukaryot Cell* 13: 1484-1493.

Wolf JM, Espadas J, Luque-Garcia J, Reynolds T, Casadevall A 2015. Lipid biosynthetic genes affect *Candida albicans* extracellular vesicle morphology, cargo, and immunostimulatory properties. *Eukaryot Cell* 14: 745-754.

Xu R, Rai A, Chen M, Suwakulsiri W, Greening DW, Simpson RJ 2018. Extracellular vesicles in cancer — implications for future improvements in cancer care. *Nature Reviews Clinical Oncology* 15: 617-638.

Yang JE, Rossignol ED, Chang D, Zaia J, Forrester I, Raja K, Winbigler H, Nicastro D, Jackson WT, et al. 2020. Complexity and ultrastructure of infectious extracellular vesicles from cells infected by non-enveloped virus. *Sci. Rep.* 10: 7939.

Zabeo D, Cvjetkovic A, Lässer C, Schorb M, Lötvall J, Höög JL 2017. Exosomes purified from a single cell type have diverse morphology. *Journal of extracellular vesicles* 6: 1329476-1329476.

Zanetti G, Briggs JAG, Grünewald K, Sattentau QJ, Fuller SD 2006. Cryo-Electron Tomographic Structure of an Immunodeficiency Virus Envelope Complex In Situ. *PLoS Pathog* 2: e83.

bioRxiv preprint doi: https://doi.org/10.1101/2020.08.17.253716; this version posted August 17, 2020. The copyright holder for this preprint (which was not certified by peer review) is the author/funder, who has granted bioRxiv a license to display the preprint in perpetuity. It is made available under aCC-BY-NC-ND 4.0 International license.

Zarnowski R, Sanchez H, Covelli AS, Dominguez E, Jaromin A, Bernhardt J, Mitchell KF, Heiss C, Azadi P, et al. 2018. Candida albicans biofilm–induced vesicles confer drug resistance through matrix biogenesis. *PLoS Biol* 16: e2006872.

Zhao K, Bleackley M, Chisanga D, Gangoda L, Fonseka P, Liem M, Kalra H, Al Saffar H, Keerthikumar S, et al. 2019. Extracellular vesicles secreted by Saccharomyces cerevisiae are involved in cell wall remodelling. *Communications Biology* 2: 305.

Geolocalisation

Juliana RIZZO	ORCID	0000-0001-5538-6471
Sarah Sze Wah WONG	ORCID	0000-0002-9440-1774
Anastasia D. GAZI	ORCID	0000-0002-2922-3625
Thibault CHAZE	ORCID	0000-0002-3615-7021
Pierre-Henri COMMERE	ORCID	0000-0002-3886-4256
Sophie NOVAULT	ORCID	0000-0001-5708-3597
Mariette MATONDO	ORCID	0000-0003-3958-7710
Gerard PEHAUD-ARNAUDET	ORCID	0000-0001-6479-9470
Lysangela R ALVES	ORCID	0000-0002-1972-2658
Robin C. MAY	ORCID	0000-0001-5364-1838
Leonardo NIMRICHTER	ORCID	0000-0001-9281-6856
Marcio L. RODRIGUES :	ORCID	0000-0002-6081-3439
Vishukumar AIMANIANDA :	ORCID	0000-0001-5813-7497
Guilhem JANBON :	ORCID	0000-0002-4788-1154

Acknowledgements

This work was supported by a CAPES COFECUB grant n°39712ZK (to GJ, MLR, LA and LN). JR was supported by the CAPES-COFECUB Franco-Brazilian Research Exchange Program (88887.357947/2019-00). SSWW was supported by CEFIPRA/ANR-DFG-AfuINF grant and Pasteur-Roux-Cantarini postdoctoral fellowship. VA was supported by ANR-DFG AfuINF and Indo-French Centre for the Promotion of Advanced Research (CEFIPRA; Grant N°5403-1) grants. Jean-Marie Winter from the NanoImaging Core at Institut Pasteur is acknowledged for his support image acquisition. The NanoImaging Core was created with the help of a grant from the French Government's 'Investissements d'Avenir' program (EQUIPEX CACSICE – "Centre d'analyse de systèmes complexes dans les environnements complexes", ANR-11-EQPX-0008). The Falcon II equipping the F20 microscope at the UBI used during

bioRxiv preprint doi: https://doi.org/10.1101/2020.08.17.253716; this version posted August 17, 2020. The copyright holder for this preprint (which was not certified by peer review) is the author/funder, who has granted bioRxiv a license to display the preprint in perpetuity. It is made available under aCC-BY-NC-ND 4.0 International license.

this study was also financed by the Equipex CACSICE (grant number ANR-11-EQPX-0008). M.L.R. is supported by grants from the Brazilian Ministry of Health (grant 440015/2018-9), Conselho Nacional de Desenvolvimento Científico e Tecnológico (CNPq; grants 405520/2018-2 and 301304/2017-3), and Fiocruz (grants VPPCB-007-FIO-18 and VPPIS-001-FIO18)MLR, JR, and FCGR also acknowledge support from Coordenação de Aperfeiçoamento de Pessoal de Nível Superior (CAPES, finance code 001) and the Instituto Nacional de Ciência e Tecnologia de Inovação em Doenças de Populações Negligenciadas (INCT-IDPN). MLR is currently on leave of an associate professor position at the Instituto de Microbiologia Paulo de Góes of the Universidade Federal do Rio de Janeiro

bioRxiv preprint doi: https://doi.org/10.1101/2020.08.17.253716; this version posted August 17, 2020. The copyright holder for this preprint (which was not certified by peer review) is the author/funder, who has granted bioRxiv a license to display the preprint in perpetuity. It is made available under aCC-BY-NC-ND 4.0 International license.

6. Figures and Legends

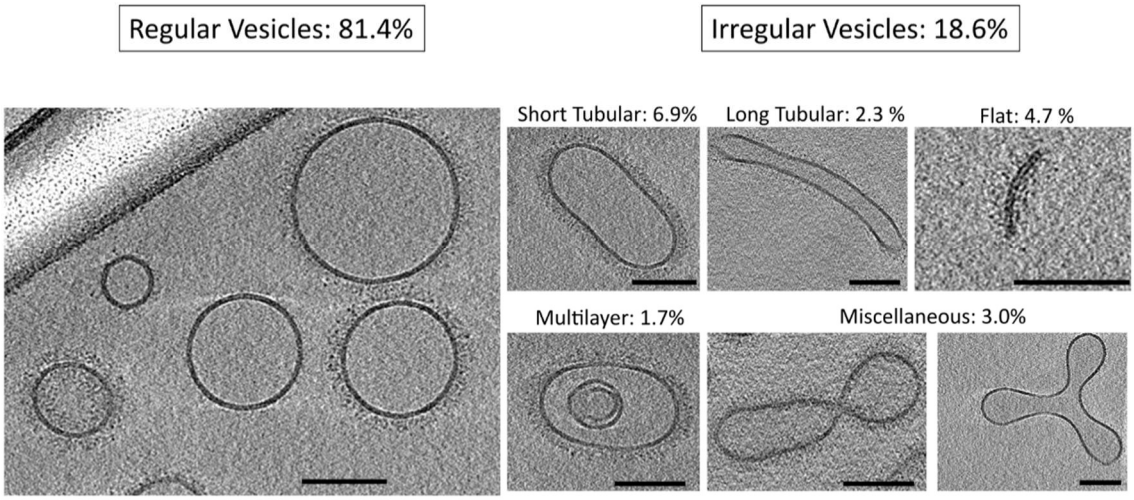

Figure 1: Gallery of EV categories. Cryo-EM analysis of 533 single EVs obtained from *C. neoformans*. EVs were characterized according to their morphological aspects in regular (rounded- bilayer vesicles) and irregular (not rounded – bilayer or multilayered vesicles) categories. Regular vesicles represented 81.4% of all EV analyzed. The irregular vesicles were subclassified as short tubular (6.9%), long tubular (2.3%), flat (4.7%), multilayer (1.7%), or vesicles with miscellaneous morphologies (3.0%). Scale bars represent 100nm.

bioRxiv preprint doi: https://doi.org/10.1101/2020.08.17.253716; this version posted August 17, 2020. The copyright holder for this preprint (which was not certified by peer review) is the author/funder, who has granted bioRxiv a license to display the preprint in perpetuity. It is made available under aCC-BY-NC-ND 4.0 International license.

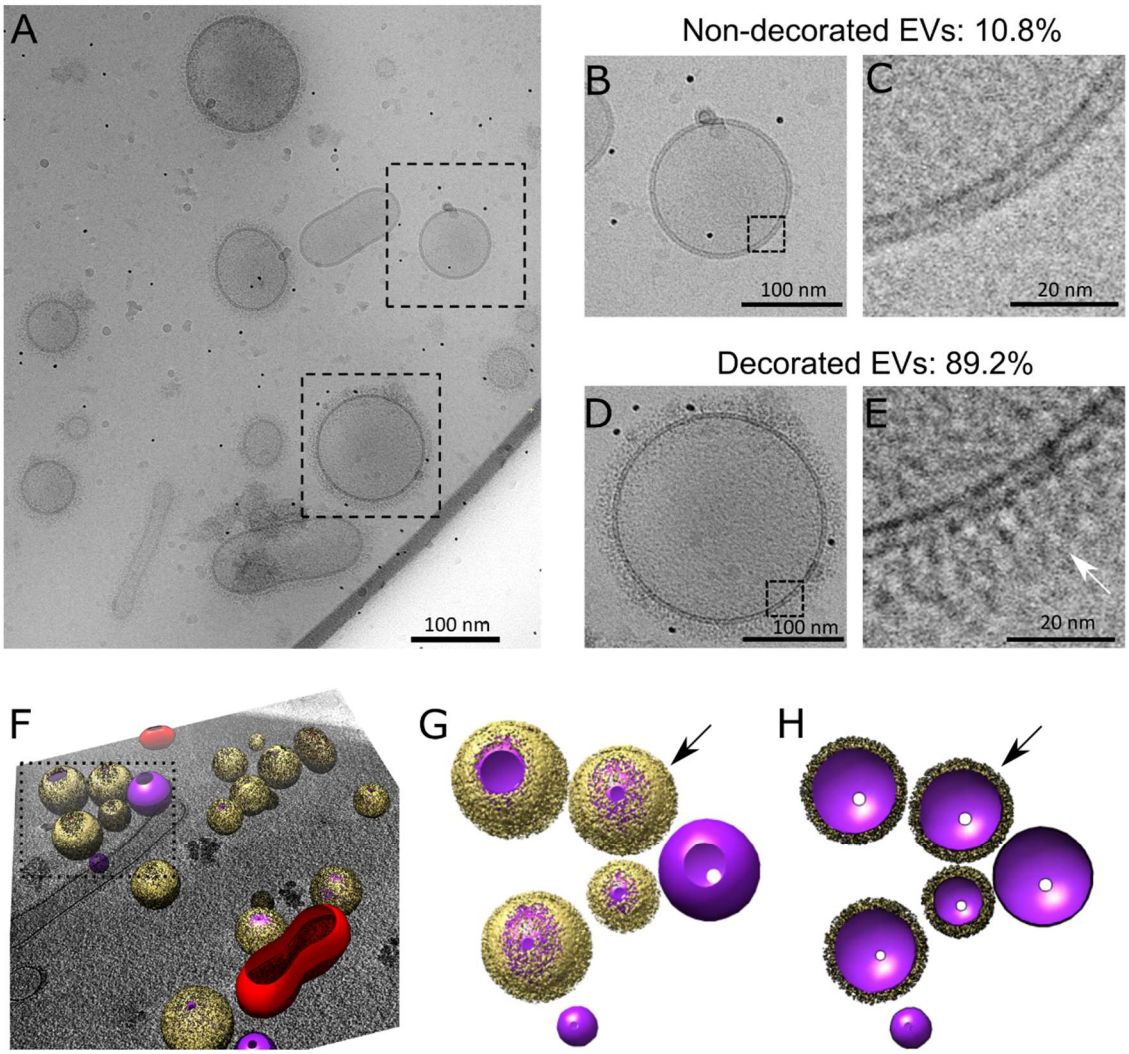

Figure 2: Cryo-electron microscopy analysis of *C. neoformans* EVs.
Cryo-EM analysis revealed a heterogeneous population of vesicles with diverse structural aspects, previously unappreciated in fungal vesicles (A). As evidenced by the magnifications, the EVs were delimitated by a lipid bilayer (B to E), which showed either no decoration (in 10.8% vesicles, panels B and C) or a fibrillar decoration (pointed by arrows) in 89.2% of the EVs analyzed (panels D and E). Three-dimensional organization of the fibrillar decoration (yellow) on the membrane (purple) of EVs as revealed by cryo-electron tomography analysis (F), magnified in the panels G and H. Full surface representation models as seen from top view (G). Same models clipped with clipping plane oriented perpendicular to line of sight (H).

bioRxiv preprint doi: https://doi.org/10.1101/2020.08.17.253716; this version posted August 17, 2020. The copyright holder for this preprint (which was not certified by peer review) is the author/funder, who has granted bioRxiv a license to display the preprint in perpetuity. It is made available under aCC-BY-NC-ND 4.0 International license.

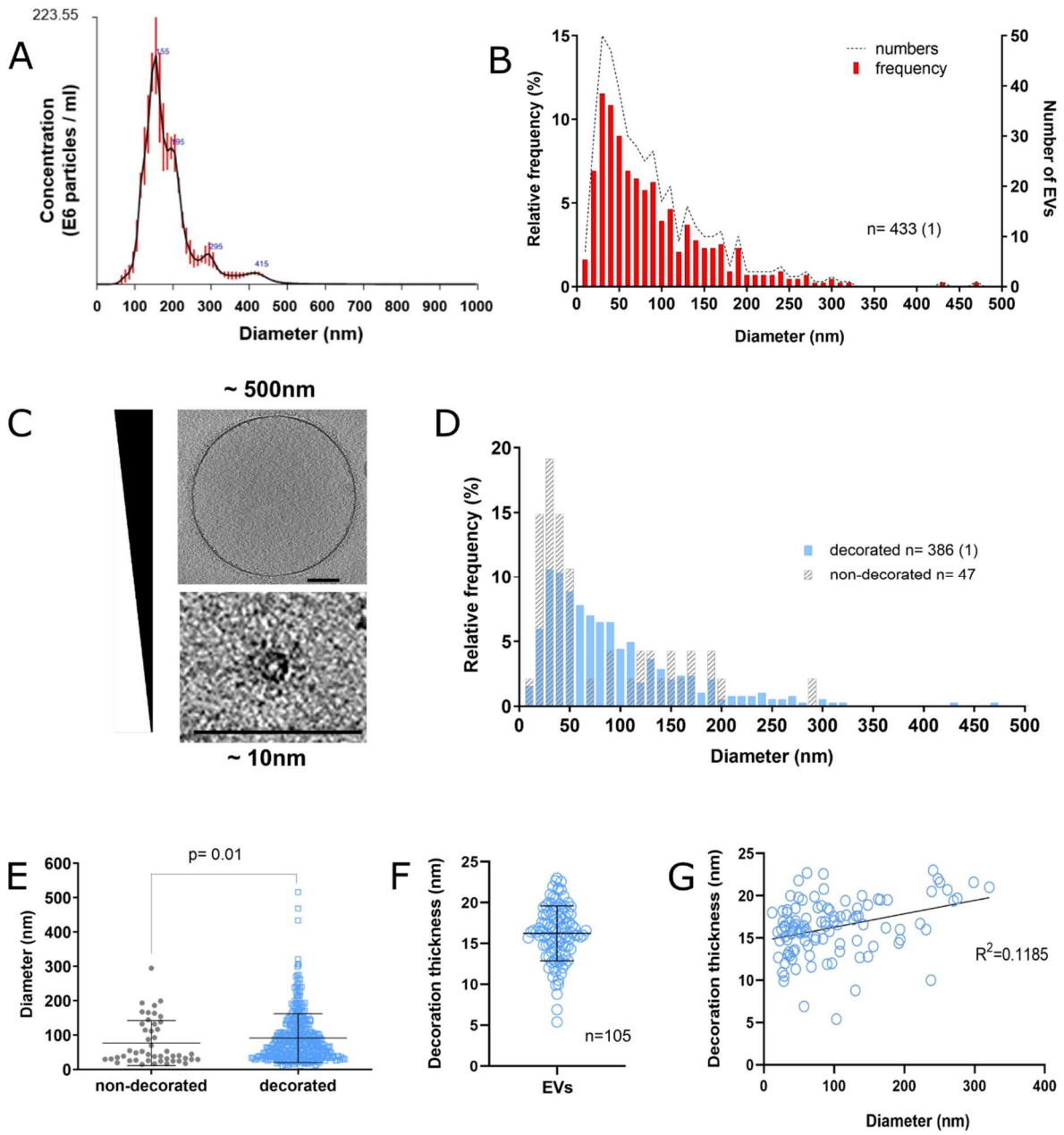

Figure 3: Analysis of size and structural diversity of *C. neoformans* EVs.
(A) NTA analysis of purified EVs revealed a size diameter ranging from 80 to 500 nm, with the highest distribution around 150 nm. (B) Frequency distribution of EV diameters determined by CryoEM, a total of 434 regular EVs were analyzed. The analysis based on CryoEM tomograms revealed a wider range of EV size distribution, from 10 to 500 nm diameter, with the highest relative frequency below 100 nm. (C) Cryo-EM images exemplifying EV size range. Scale bars corresponding to 100 nm. (D) EV size distribution according to the presence or absence of surface decoration. (E) Non-decorated EVs have a smaller diameter size distribution compared to decorated ones. (F) Analysis of decoration thickness from Cryo-EM images from 105 single EVs. (G) Analysis of a potential relationship between decoration thickness and EV diameter by linear regression. Error bars are represented as means ± SD. Sample size (n) is indicated and, in brackets, the number of vesicles in that category that exceeded 500 nm in size.

bioRxiv preprint doi: https://doi.org/10.1101/2020.08.17.253716; this version posted August 17, 2020. The copyright holder for this preprint (which was not certified by peer review) is the author/funder, who has granted bioRxiv a license to display the preprint in perpetuity. It is made available under aCC-BY-NC-ND 4.0 International license.

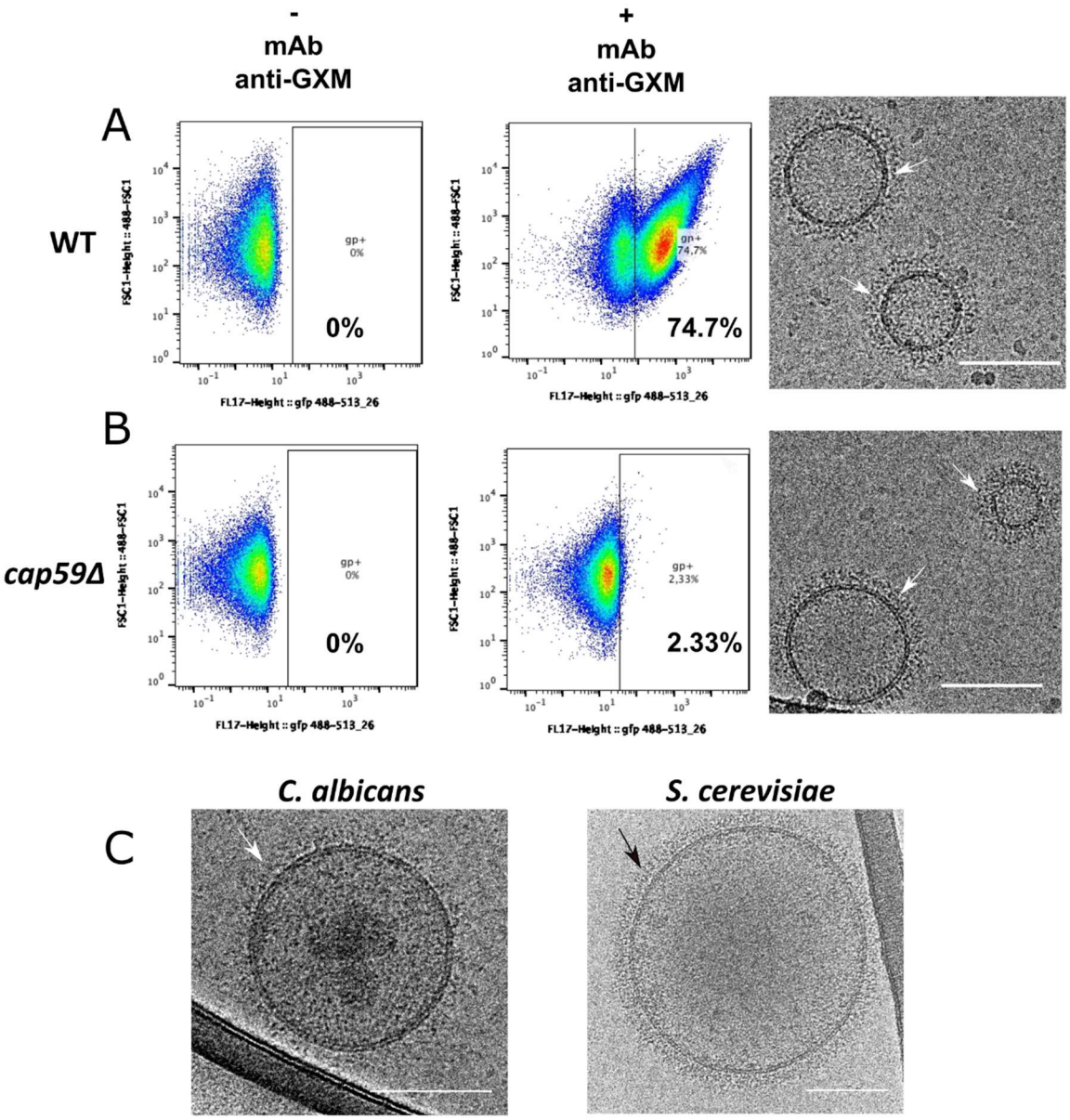

Figure 4: Flow cytometry analysis of *C. neoformans* EVs incubated with anti-GXM monoclonal antibody.

FACS analysis of WT and the acapsular *cap59Δ* EVs in PBS or in the presence of the monoclonal antibody raised against the capsular polysaccharide 18b7 (+ mAb anti-GXM). (A) The analysis revealed strong labeling of WT vesicles (74.7%), compared to the weak labeling in the mutant (2.33%), (B). Despite the important labeling difference, *C. neoformans* WT and *cap59Δ* strains released EVs bearing similar surface decoration, shown by the cryo-EM (arrows), as well as EVs obtained from other fungal species such as *C. albicans* and *S. cerevisiae* (C). Scale bar represents 100 nm. This experiment was repeated two times with similar results.

bioRxiv preprint doi: https://doi.org/10.1101/2020.08.17.253716; this version posted August 17, 2020. The copyright holder for this preprint (which was not certified by peer review) is the author/funder, who has granted bioRxiv a license to display the preprint in perpetuity. It is made available under aCC-BY-NC-ND 4.0 International license.

A

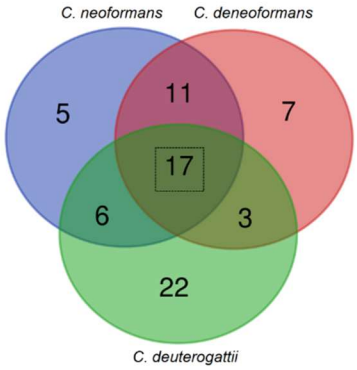

B

List of EV- associated proteins shared by the three *Cryptococcus spp.*

C. deuterogattii	*C. deneoformans*	*C. neoformans*	Putative name	Putative function
CNBG_1155	CNA07540	CNAG_00776	MP88	MP88, immunoreactive mannoprotein MP88
CNBG_3648	CNC06180	CNAG_03007	CPC1	DUF3759
CNBG_3432	CNC03950	CNAG_02775	VEP2	GPI anchored protein
CNBG_9064	CND03490	CNAG_01230	MP98/CDA2	MP98, chitin deacetylase 2
CNBG_5182	CNE05040	CNAG_02030	GOX2	glyoxal oxidase
CNBG_3374	CNC03380	CNAG_01854	HEP2	heparinase II/III family protein
CNBG_1745	CNF01800	CNAG_05799	CDA1	Chitin deacetylase
CNBG_4970	CNN02260	CNAG_06501	GAS1	1,3-beta-glucanosyltransferase
CNBG_5817	CNJ03160	CNAG_04891	RIL1	Ricin-type beta-trefoil lectin domain containg protein
CNBG_4258	CNH02560	CNAG_05615	SSO1	t-SNARE complex subunit
CNBG_9173	CNF01900	CNAG_05788	VMA10	V-type ATPase, G subunit
CNBG_5332	CNE03480	CNAG_02189	AMY1	Alpha-amylase
CNBG_4145	CNE01150	CNAG_02443	VEP3	NADH dehydrogenase
CNBG_5365	CNE03150	CNAG_02225	EXG104	EXG104, glucan 1,3-beta-glucosidase
CNBG_0679	CND02350	CNAG_01109	VEP4	hypothetical protein
CNBG_0806	CND03580	CNAG_01239	CDA3	CDA3, Chitin deacetylase
CNBG_5038	CNN01470	CNAG_06422	VEP5	hypothetical protein

C

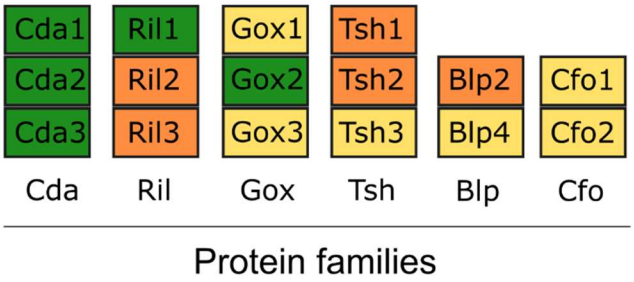

D

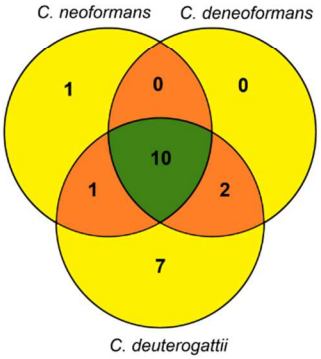

Figure 5: Analysis of *Cryptococcus spp* protein cargo.
(A) Venn diagram revealing the EV-associated proteins overlap among *C. neoformans*, *C. deneoformans*, and *C. deuterogattii*. Seventeen proteins were identified to be associated with EVs in all three *Cryptococcus* species (B) List of the gene loci and the corresponding proteins commonly found in EVs released by the three species, which could be considered as putative cryptococcal EV-protein markers. Most of the proteins are predicted to be GPI anchor protein, to contain a signal peptide or to possess other membrane domains, according to preGPI, signalP and TMHMM website, respectively. (C) Six protein families appeared to be typical of *Cryptococcus* EVs, including the Chitin deactelylase family (Cda), the Ricin-type beta-trefoil lectin domain-containing protein family (Ril), the putative glyoxal oxidase family (Gox), the tetraspanin membrane proteins containing a SUR7/PalI family motif (Tsh), the pr4/barwin domain protein family (Blp), and the multicopper oxidase (Cfo). Among these families, the proteins present in all three species are shown in green, proteins present in two species in orange) and proteins present in only one species in yellow. (D) We also identify 21 putative GPI-anchored proteins, as predicted by PredGPI, and 10 of them were present in all three species.

bioRxiv preprint doi: https://doi.org/10.1101/2020.08.17.253716; this version posted August 17, 2020. The copyright holder for this preprint (which was not certified by peer review) is the author/funder, who has granted bioRxiv a license to display the preprint in perpetuity. It is made available under aCC-BY-NC-ND 4.0 International license.

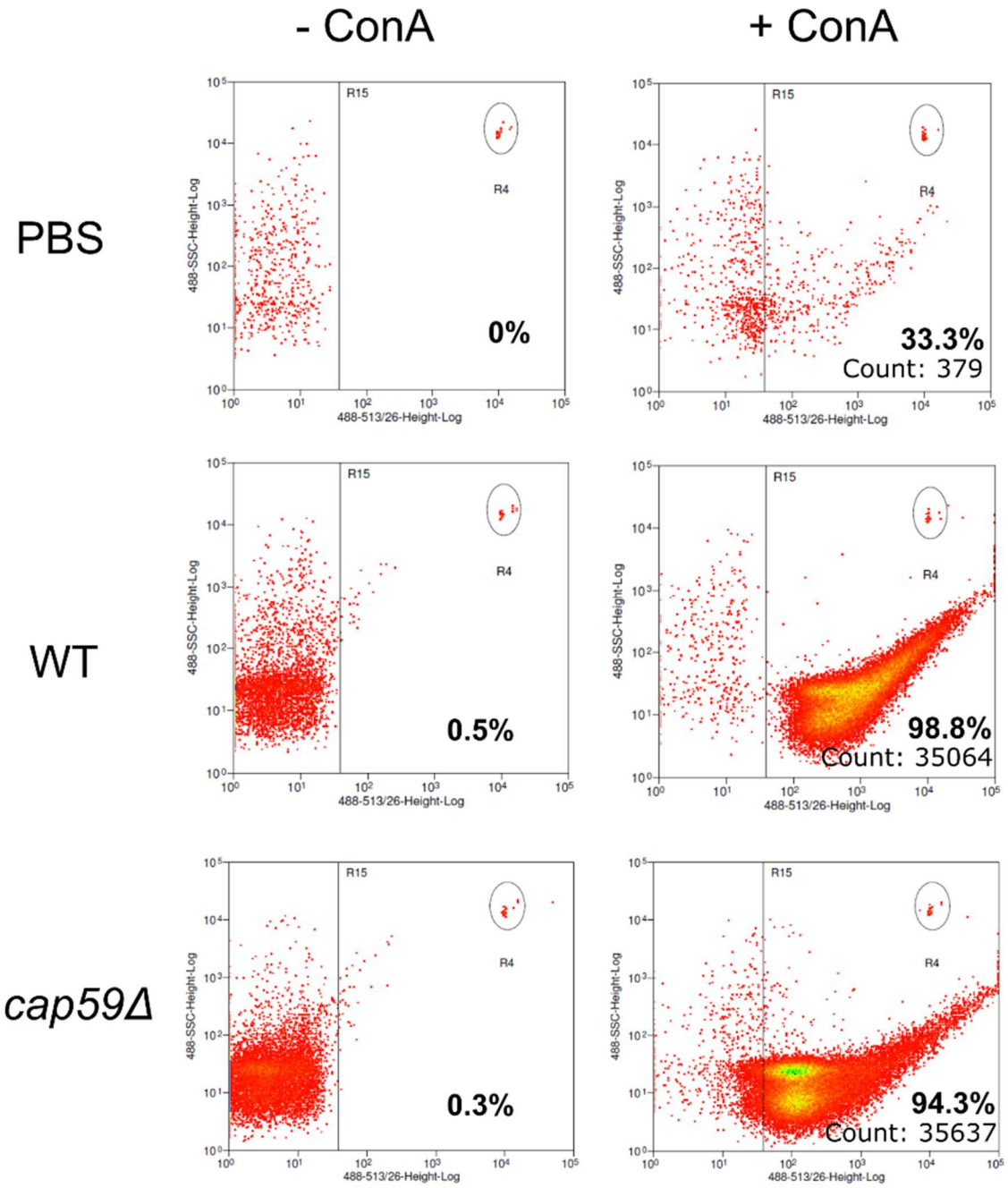

Figure 6. Flow cytometry analysis of *C. neoformans* EVs incubated with GFP-labelled ConA.

FACS analysis of EVs obtained from WT and *cap59Δ* cells. EVs were incubated with ConA-Alexa Fluor 488 conjugated lectin and mixed in BD Trucount tubes (BD Biosciences), contained a known number of fluorescent beads. The number of beads for each reading was fixed to 50 (gate R4), and the percentage of ConA labeling and the number of labeled particles (count) were recorded. This experiment was repeated three times with similar results.

bioRxiv preprint doi: https://doi.org/10.1101/2020.08.17.253716; this version posted August 17, 2020. The copyright holder for this preprint (which was not certified by peer review) is the author/funder, who has granted bioRxiv a license to display the preprint in perpetuity. It is made available under aCC-BY-NC-ND 4.0 International license.

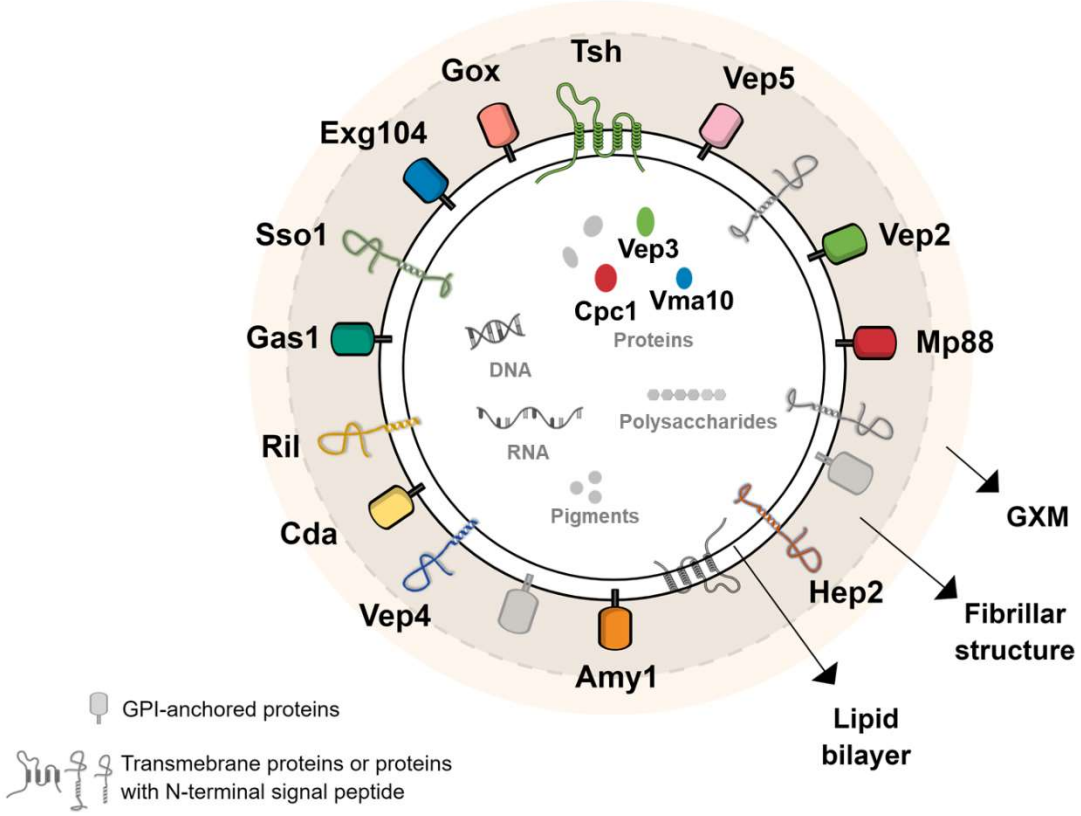

Figure 7: Model of simplified molecular structure and composition of *Cryptococcus* EVs.

In accordance to previous reports and in the light of our data, a new model of *Cryptococcus* EVs is suggested, where the outer layer is composed by the capsular polysaccharide glucuronoxylomannan (GXM), and the lipid bilayer is covered by many proteins, including mannoproteins, making the visual fibrillar structure resolved by cryo-EM. Most of the proteins are predicted to be GPI-anchored, to contain a signal peptide or to possess other membrane domains, according to preGPI, signalP and TMHMM, respectively. Three proteins the hypothetical protein Cpc1, the putative V-type ATPase (Vma10) and the Vep3 are predicted to be soluble. It is still unclear if these proteins are indeed inside the vesicular lumen or linked to any other transmembrane protein. For simplification, the lipid content was not explored, but previous works shown the presence of sterol, phospholipoids and sphingolipids. Additionally, *Cryptococcus* EVs were also described to contain other cargoes, such as DNA, RNA, pigments and polysaccharides, including GXM, as detailed in plain text.

bioRxiv preprint doi: https://doi.org/10.1101/2020.08.17.253716; this version posted August 17, 2020. The copyright holder for this preprint (which was not certified by peer review) is the author/funder, who has granted bioRxiv a license to display the preprint in perpetuity. It is made available under aCC-BY-NC-ND 4.0 International license.

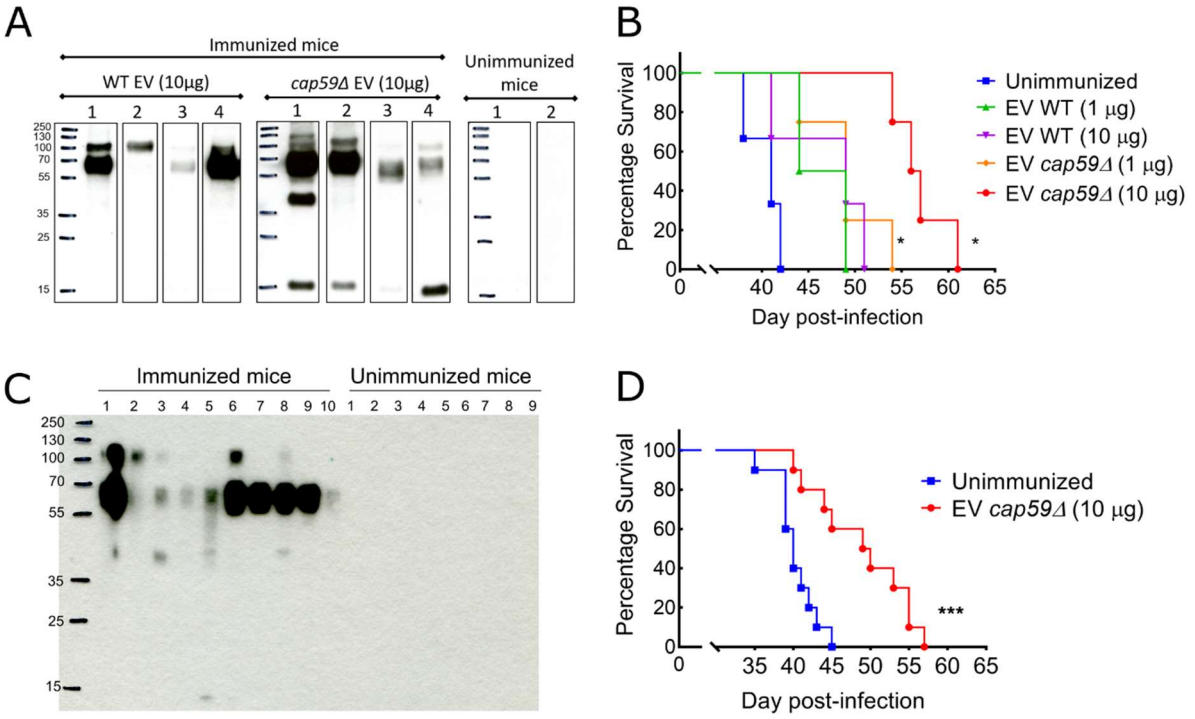

Figure 8. Vaccination assays using *C. neoformans* EVs.

BALB/c mice of 6 weeks were firstly immunized with *C. neoformans* EVs via intraperitoneal injection, after infected intranasally with 1 x 10^4 WT cells and the mice survival was finally monitored. (A) In the first pilot experiment, mice (n = 4 per group) were immunized three times with EV from WT, and *cap59Δ* strains (EV-associated protein extract of 1 µg/100 µL or 10 µg/100 µL in PBS) and control mice were injected with 100 µL PBS. Western Blot using mice sera against fungal EV confirmed that all immunized mice produced antibodies against vesicular components. (B) All EV-immunized mice survived longer than the non-immunized ones, but the immunization with *cap59Δ* EVs rendered the significantly prolonged mice survival (*p=0.01). (C) For the second experiment, mice (n=10 per group) were immunized five times uniquely with EV obtained from *cap59Δ* strain (EV-associated protein extract of 10 µg/100 µL in PBS) and control mice were injected with 100 µL PBS. Again, Western blot using mice sera against fungal EV confirmed that all immunized mice produced antibodies against EV components. (D) EV-immunized mice showed a higher significant prolonged survival (*p=0.0006), compared to the unimmunized group. The comparison of the survival curves was made by GraphPad Prism 8, using the Log-rank (Mantel-Cox) test.